JOURNAL OF PETROLOGY | VOLUME 41 | NUMBER 9 | PAGES 1365–1396 | 2000

Identifying Accessory Mineral Saturation during Differentiation in Granitoid Magmas: an Integrated Approach

PAUL W. O. HOSKIN[1]*, PETER D. KINNY[2], DOONE WYBORN[3] AND BRUCE W. CHAPPELL[3]

[1]RESEARCH SCHOOL OF EARTH SCIENCES, AUSTRALIAN NATIONAL UNIVERSITY, CANBERRA, A.C.T. 0200, AUSTRALIA

[2]TECTONICS SPECIAL RESEARCH CENTRE, SCHOOL OF APPLIED GEOLOGY, CURTIN UNIVERSITY OF TECHNOLOGY, GPO BOX U1987, PERTH, W.A. 6001, AUSTRALIA

[3]DEPARTMENT OF GEOLOGY, AUSTRALIAN NATIONAL UNIVERSITY, CANBERRA, A.C.T. 0200, AUSTRALIA

RECEIVED OCTOBER 4, 1999; REVISED TYPESCRIPT ACCEPTED JANUARY 25, 2000

Numerical reconstructions of processes that may have operated during igneous petrogenesis often model the behaviour of important trace elements. The geochemistry of these trace elements may be controlled by accessory mineral saturation and fractionation. Determination of the saturation point of accessory minerals in granitoid rocks is ambiguous because assumptions about crystal morphology and melt compositions do not always hold. An integrated approach to identifying accessory mineral saturation involving petrography, whole-rock geochemical trends, saturation calculations and mineral chemistry changes is demonstrated here for a compositionally zoned pluton. Within and between whole-rock samples of the Boggy Plain zoned pluton, eastern Australia, the rare earth element (REE)-enriched accessory minerals zircon, apatite and titanite exhibit compositional variations that are related to saturation in the bulk magma, localized saturation in intercumulus melt pools and fractionation of other mineral phases. Apatite is identified as having been an early crystallizing phase over nearly the whole duration of magma cooling, with zircon (and allanite) only saturating in more felsic zones. Titanite and monazite did not saturate in the bulk magma at any stage of differentiation. Although some trace elements (P, Ca, Sc, Nb, Hf, Ta) in zircon exhibit compositional variation progressing from mafic to more felsic whole-rock samples, normalized REE patterns and abundances (except Ce) do not vary with progressive differentiation. This is interpreted to be a result of limitations to both simple 'xenotime' and complex xenotime-type coupled substitutions. Our data indicate that zircon REE characteristics are not as useful as those of other REE-rich accessory minerals as a petrogenetic indicator.

KEY WORDS: *saturation; zircon; apatite; titanite; magma differentiation; trace elements; REE patterns*

INTRODUCTION

Accessory minerals typically compose less than one modal percent of a whole-rock sample, yet host significant fractions of the whole-rock budget of important trace elements and isotopes (Gromet & Silver, 1983; Bea, 1996; Vervoot *et al.*, 1996). One mineral in particular, zircon, has become an invaluable 'stop-off point' on the journey of investigation into crustal evolution because of its stability, internal textures and extremely high U/Pb ratio at crystallization (Buick *et al.*, 1995; Hanchar & Rudnick, 1995; Bowring *et al.*, 1998; Bowring & Williams, 1999). Zircon and other common accessory minerals (apatite, monazite and allanite) have been intensively studied in natural and experimental systems to understand their behaviour and effects upon igneous processes, and specifically upon the behaviour of the rare earth elements (REE).

*Corresponding author. Present address: Department of Geological Sciences, University of Canterbury, Private Bag 4800, Christchurch 8020, New Zealand. Fax: +64 3 341 0100. E-mail: Papanui@xtra.co.nz

Extended data set can be found at: http://www.petrology.oupjournals.org

© Oxford University Press 2000

The control exercised by accessory minerals on the REEs in natural systems is highlighted by the mass-balance approach to modelling of igneous melting–crystallization–assimilation processes. In many cases a satisfactory numerical 'solution' to major-element modelling of a particular process cannot reproduce the changes in REE abundances measured in the rock samples. An assumption of trace element behaviour for mass-balance purposes is that the modelled element must be essentially contained within major rock-forming minerals (i.e. not accessory minerals) and obey Raoult–Henry's Law. Because these two assumptions are violated for the case of the REE, Bea (1996) concluded that the REE (and Y, Th and U) cannot be used for modelling the genesis of granitoids.

Although in principle the conclusion of Bea (1996) is correct, in practice the REEs can still be a powerful tool in mass-balance modelling by the addition of high-REE-K_d accessory minerals to a model mineral assemblage. This has very little effect on the major-element mass balance, but a significant effect on the REE. Taylor *et al.* (1995) closely reproduced measured light REE (LREE) abundances in a suite of alkaline volcanics by including allanite in their mass-balance calculations, although this phase was selected instead of apatite and monazite, which also occur in their samples, without knowledge of the saturation behaviour of allanite. The inclusion of a particular accessory mineral in a model assemblage must be constrained by a knowledge of what minerals were saturated in the bulk magma. Petrographic evidence that might provide such a constraint is generally lacking in granitoid rocks, and it is probable that most granitoid samples represent a mix of (cumulate and restitic) minerals and melt, not simply a solidified melt. This consideration alone may introduce large uncertainties into saturation calculations for accessory minerals based on experimental studies by Watson and others (Harrison & Watson, 1983, 1984; Watson & Harrison, 1983; Montel, 1986; Rapp & Watson, 1986). Moreover, it is not possible to unambiguously identify an accessory mineral as being early crystallized based on euhedral morphology, because a phase that begins to crystallize with only a small fraction of melt remaining can still be euhedral and included in a major rock-forming mineral.

To reduce the difficulty of identifying the saturation point of an accessory phase, Evans & Hanson (1993) demonstrated an 'inverse' modelling approach for a cogenetic sample suite. By this approach the saturation behaviour of an accessory mineral is determined from the variation trend of a mineral's essential structural constituent (ESC; e.g. P in apatite) in the bulk-rock chemistry across the suite as a function of differentiation. Evans & Hanson (1993) illustrated the role of zircon saturation in the differentiation of a suite of calc-alkaline lavas from Batopilas, Mexico, contradicting Cameron & Hanson (1982), who argued against zircon involvement from whole-rock Zr/Nd ratios. 'Inverse' modelling becomes ambiguous when more than one accessory phase having identical ESCs saturate at approximately the same degree of differentiation (e.g. LREE in allanite and monazite, or P in xenotime and apatite), or when a major rock-forming mineral affects the behaviour of an accessory mineral's ESC and 'masks' the saturation point of that accessory mineral (e.g. Ti in biotite masking the saturation point of titanite on a plot of whole-rock TiO_2 vs differentiation index).

A problem with the 'inverse' modelling approach in identifying the role of accessory phases in magmatic differentiation is the effects of localized saturation and crystallization of accessory phases adjacent to growing rock-forming minerals. These phases form within non-equilibrium concentration gradients and can be included in fractionating phases such as feldspar and pyroxene (Bacon, 1989). Fractionation of accessory phases in this manner can affect the REE chemistry of the melt (even if only slightly). In such cases 'inverse' modelling and saturation calculations will suggest that saturation has not been attained in a particular sample, thus this phase would not be included in mass-balance calculations.

For granitoid rocks much of the ambiguity involved with identifying which accessory phase(s) was important in REE fractionation at a particular point of differentiation would be reduced if it could be demonstrated that the REE chemistry of the accessory minerals themselves preserves evidence of the saturation behaviour of other phases. In the case of apatite, for example, the previous crystallization of monazite could be recorded in the apatite normalized REE pattern by a relative reduction of the LREE abundances. This reasoning is analogous to the effects that crystal fractionation is interpreted to have on a melt; for example, a melt that has experienced calcic-feldspar fractionation will exhibit Eu depletion. This approach would be especially useful for intermediate to high-silica suites that demonstrate REE depletion with increasing fractionation, but where 'inverse' modelling and textural relations are ambiguous.

Changes in the chemical composition of accessory minerals have previously been investigated for samples from two plutons in California, USA (Sawka, 1988; Wark & Miller, 1993). These studies revealed that the chemistry of accessory minerals not only controlled much of the trace element chemistry of the plutons, but in a general way also recorded changes in melt composition that occurred during differentiation. This study investigates chemical changes in selected REE-enriched accessory minerals from the Boggy Plain zoned pluton that may have resulted from the fractionation of other, earlier crystallizing accessory phases. This information is integrated with 'inverse' modelling and saturation calculations to unambiguously identify which accessory

phases were important fractionating phases at various stages of differentiation within the Boggy Plain magma. Unambiguous identification is important to constrain models of magmatic differentiation. We further look at the chemistry of accessory phases to access their widespread usefulness as petrogenetic indicators and explain the REE chemistry of zircon.

THE BOGGY PLAIN ZONED PLUTON

Field relations and description

The Boggy Plain zoned pluton (BPZP) is located in the southeastern part of the Lachlan Fold Belt (148°35′E, 35°52′S), eastern Australia, and forms part of the Boggy Plain Supersuite, which extends for >500 km in the central Lachlan Fold Belt. The BPZP has been described in detail by Wyborn (1983), Wyborn *et al.* (1987) and Wyborn & Chappell (2000). The pluton comprises concentric zones of various rock types and crops out over 36 km^2 as flat rock pavements and tors up to 10 m high. The pluton intrudes Ordovician (Boltens beds) and Early Silurian (Tantangara Formation) deep marine sediments, and a Late Silurian garnet-bearing granitoid (Gang Gang Adamellite). An intense contact metamorphic aureole was developed, discernible up to 2 km from the contact with the BPZP. The pluton has been faulted into two sectors by the Boggy Plain Fault, along which there has been ~4·9 km of left lateral strike-slip and a small component of dip-slip. Map reconstruction of the pluton reveals good correlation of rock types across the fault (Fig. 1).

Volumetrically, BPZP outcrop is dominated by adamellite (70% of total area) and granodiorite (25%), as seen in Fig. 1. Other zones contain diorite, quartz monzodiorite and aplite. Rock compositions span a SiO_2 range of 50–75 wt %. Contacts between rock types vary from gradational (diorite–granodiorite) to sharp (granodiorite–adamellite). The adamellite–aplite contact is not exposed. The six whole-rock samples selected for this study represent each major zone and rock type present, except for bodies of quartz monzodiorite and diorite at the southern margin of the pluton, which are interpreted as separate intrusions (Wyborn, 1983).

The major, rock-forming minerals for each sample are described here. Accessory mineral occurrences are described in the following section. Mineral abundances (in area %) were determined on polished rock slabs (200 cm^2) by point-counting using a 2 mm grid, and thin-section point-counting using a 0·5 mm grid (Wyborn, 1983). Errors were estimated according to Bayly (1965). Sample BP39 is a dark, fine-grained, quartz-bearing diorite, with a distinctive foliation defined by unzoned plagioclase ($An_{60–65}$) and pyroxene crystals. Alumina-poor orthopyroxene (*mg*-number 56–72) and Ti-poor clinopyroxene (*mg*-number 67–85) comprise 32 ± 2% of the rock. Olivine (*mg*-number 64–65) is a minor phase in the diorites and is usually altered. Quartz, biotite, hornblende and orthoclase are minor, interstitial phases. Samples from the granodiorite (BP7 and BP16) contain euhedral, zoned plagioclase ($An_{30–55}$), subhedral clinopyroxene (*mg*-number 69–83, BP7), and orthopyroxene (*mg*-number 58–73) as major mineral phases. Hornblende, quartz and orthoclase are significant interstitial phases. Biotite is a minor interstitial phase. The granodiorite zone can be separated into two distinct sub-zones on the basis of whole-rock [MgO + FeO_{Total}] and modal mineralogy; the inner granodiorite (BP16), although mineralogically similar to the outer granodiorite (BP7), contains more plagioclase and opaques, less orthoclase and pyroxenes, and its hornblende exhibits a different habit and chemistry. Hornblende in BP16 crystallized at higher temperatures than in BP7 (on the basis of Na + K and Ti contents) as a result of higher fH_2O stabilizing calcic-amphibole over pyroxene at relatively higher temperatures. In the adamellite (defined here as a rock in which alkali-feldspar is between 35 and 65% of total feldspar), euhedral hornblende and biotite join plagioclase and quartz as major phases. All adamellite samples contain some plagioclase crystals with cores of $An_{55–60}$, although crystals of $An_{30–35}$ are typical in the outer adamellite (BP22) and An_{20} in the inner adamellite (BP11). Clinopyroxene (*mg*-number 72–80) is a minor (2 ± 1%) phase in BP22. Perthitic orthoclase, up to 4 mm long, is interstitial in BP22, but is both an early crystallizing and interstitial phase in the inner adamellite (BP11). Sample BP42 is a hornblende-free, fine- to medium-grained aplite, comprising quartz, perthitic orthoclase, strongly zoned plagioclase ($An_{15–55}$), and biotite. Clinopyroxene (*mg*-number 67–74) is rare or absent from most aplite samples.

In the field, areas of low-temperature alteration are discernible within the granodiorite by rock discoloration and an angular, blocky outcrop pattern contrasting with adjacent unaltered rocks. There is no macroscopic evidence of high-temperature (~700°C) hydrothermal alteration, which has affected the central aplites and surrounding adamellite. Evidence for a hydrothermal fluid is derived from accessory mineral occurrences, textures and chemistry (Wyborn, 1983; Hoskin *et al.*, 1998). The REE-rich hydrous fluid, which probably evolved from the magma at the final stages of differentiation, is responsible for the pervasive alteration or replacement of magmatic accessory phases (apatite, titanite, magnetite) and the crystallization of hydrothermal phases (scheelite, ilmenite, rutile, yttrobetafite, zircon).

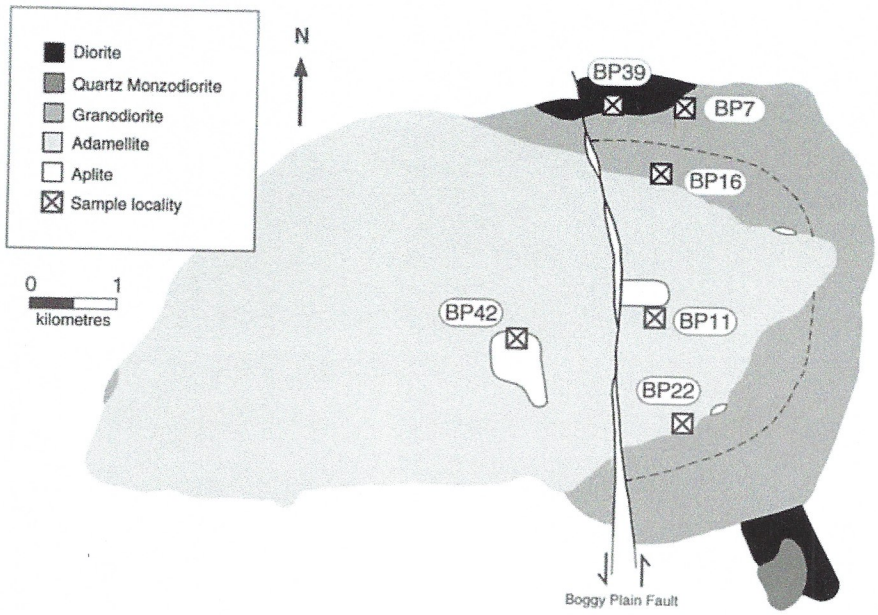


Fig. 1. Simple geological map of the Boggy Plain zoned pluton, New South Wales, Australia. The map has been constructed by subtracting 4·9 km of left-lateral strike-slip along the Boggy Plain Fault. The dashed line divides the granodiorite on the basis of MgO + FeO_{Total} into the inner and outer granodiorite. Localities of samples used in this study are denoted by a crossed-box symbol with the sample label given. [After Wyborn (1983).]

Accessory mineral occurrences

A variety of magmatic accessory phases are observed in thin-section and mineral separates from samples throughout the pluton (Table 1). Zircon occurs throughout the BPZP as euhedral prismatic crystals up to 600 μm in length, except in BP39 (diorite), where the crystals are commonly anhedral to subhedral and equant (~150 μm). In the diorite, zircon is interstitial to surrounding plagioclase crystals, and in the granodiorite it is commonly found included in interstitial biotite. In the adamellite and aplite, zircon is distributed throughout the rock. Cathodoluminescence (CL) imaging reveals zircon to have oscillatory zoning in all occurrences. CL imaging shows inherited zircon cores in some zircons from the granodiorite, adamellite and aplite; most crystals from BP16 (inner granodiorite) contain large, round cores. The zoning characteristics of zircon in the BPZP have been described in detail by Hoskin (2000).

Apatite is also an accessory phase in all rocks of the BPZP, occurring as intergranular tabular crystals up to 1 mm long and as acicular inclusions (up to 300 μm long) in most major mineral phases. These acicular inclusions probably formed at the crystal–melt interface during phenocryst growth by local saturation (Bacon, 1989). Some crystals from BP11 (inner adamellite) and BP42 (aplite) are weakly pleochroic (purplish blue–pale pink). CL imaging of tabular crystals reveals broad oscillatory zoning in some crystals.

Allanite occurs as yellowish brown subhedral–euhedral tabular crystals in all samples, except from the diorite. In the granodiorite and aplite zones, euhedral allanite crystals reach 200 μm long and in the adamellite 1·5 mm long. Anhedral crystals are more common than euhedral crystals in the granodiorite. Allanite is most abundant in relatively mafic samples of the outer adamellite (BP22). Electron microprobe analyses of allanite from BP22 (outer adamellite) and BP42 (aplite) show it to be relatively Ce enriched (9–10 wt % Ce_2O_3) and Th poor (0·7–1·0 wt % ThO_2).

Ilmenite occurs as euhedral crystals (up to 150 μm long) in the diorite and granodiorite zones. It is most abundant in the diorite, but is very rare in the inner granodiorite. In these rocks it occurs predominantly as inclusions in biotite or hornblende, as separate crystals, or intergrown with magnetite. In more felsic rocks of the BPZP, titanite occurs as the principal Ti-bearing phase in the place of ilmenite. Both phases occur in rocks from the granodiorite zone, but anhedral titanite (up to 100 μm across) is interstitial and rare. Titanite occurs throughout the adamellite zone as an anhedral interstitial phase, or in the inner adamellite (BP11) as subhedral–euhedral crystals intergrown with interstitial orthoclase, where grain length can be up to 300 μm. Titanite is most abundant in the inner adamellite, but does not occur in the aplite as a result of replacement by hydrothermal ilmenite. Secondary titanite, formed by partial breakdown

Table 1: Magmatic accessory minerals in whole-rock samples from the Boggy Plain zoned pluton

Sample:	BP39	BP7	BP16	BP22	BP11	BP42
Zone:	diorite	outer granodiorite	inner granodiorite	outer adamellite	inner adamellite	aplite
Zircon	□*	■	■	■	■	■
Monazite					□	□
Allanite		□/■	□/■	■	■	■
Apatite	■	■	■	■	■	■
Magnetite	■	■	■	■	■	■
Titanite		□	□	□	□/■	†
Ilmenite	■	■	■			†

■, euhedral crystal forms; □, anhedral to subhedral crystal forms; interstitial.
*This rock may also contain baddeleyite (monoclinic ZrO_2).
†Titanite has been reacted out of this rock by W-bearing hydrothermal fluids, and ilmenite reappears as the Ti-bearing phase, possibly according to the reaction
$3CaTiSiO_5 + Fe_3O_4 + 3H_2WO_4 = 3CaWO_4 + FeTiO_3 + 3SiO_2 + 3H_2O + 1/2O_2$.

of hornblende, is present throughout the granodiorite and adamellite. It is distinguished from magmatic titanite by its occurrence and distinctly sinuous REE pattern and is not considered in this study. The change from ilmenite to titanite as the principal Ti-bearing phase corresponds to an increase in fO_2 and at no stage can both phases be considered to have crystallized simultaneously. CL and backscattered electron imaging of magmatic titanite revealed scattered patches of relatively bright luminescence and minor internal zoning.

Magnetite increases in abundance relative to mafic silicate phases across the pluton. In BP39 (diorite) it occurs as equant crystals (100–150 μm) throughout the rock and commonly as inclusions in plagioclase with ilmenite. A similar pattern of occurrence is observed in the granodiorite and adamellite zones, but in these rocks magnetite also occurs as inclusions in biotite and hornblende. In the case of hornblende, the magnetite is likely to be a breakdown product of clinopyroxene. Disseminated euhedral magnetite in the adamellite is commonly ~300 μm across. Sub-solidus re-equilibration of magnetite is apparent from the occurrence of ilmenite (plus other phases) exsolution lamellae within crystals and micro-crystals on the grain boundary. Electron microprobe analyses of magnetite from different zones indicate that V_2O_3 contents are unaffected by this re-equilibration and that a systematic decrease in abundance from mafic to felsic samples is preserved.

Monazite is an uncommon accessory phase in the adamellite and aplite zones, where it occurs as yellowish grey subhedral crystals up to 200 μm long. Its presence in all parts of the adamellite is unconfirmed. Electron microprobe analyses of monazite from BP42 (aplite) show it to be relatively Ce enriched (31 wt % Ce_2O_3) and La and Th depleted (16 wt % La_2O_3; 2 wt % ThO_2).

A single dark brown–black crystal was tentatively identified as baddeleyite in a crushed sample of BP39 (diorite). Pyrite is a common accessory mineral throughout the pluton and is sometimes associated with rare chalcopyrite. Other magmatic phases such as thorite, xenotime, aeschinite, etc., sometimes found in plutonic rocks (Schaltegger & Krähenbühl, 1990; Bea, 1996), were not observed in BPZP thin-sections or mineral separates.

Petrogenesis

Summary of whole-rock compositional variation in the BPZP

All whole-rock data presented in this study are from Wyborn (1983); analysis was by X-ray fluorescence (XRF) and instrumental neutron activation analysis (INAA). From the diorite (represented in this study by BP39), an inwardly decreasing abundance of [MgO + FeO_{Total}] continues through the granodiorite and adamellite into the aplitic core. The decrease in the adamellite is gradational (cryptic zoning), with the outer rocks containing >8 wt % and inner rocks containing <3 wt % [MgO + FeO_{Total}]. The change in rock type from marginal diorite to central aplite corresponds to decreasing TiO_2, FeO, MgO, CaO, P_2O_5, K/Rb, Sr, Sc, V, Cr, Ni, Mn, Co, Cu and Zn, and increasing SiO_2, Fe^{3+}/Fe^{2+}, K_2O, Rb, Cs, Pb, Nb, Ta and LREE abundances (Fig. 2). Distinct trends are observed for some elements. Alumina and Na_2O increase from the margin to the centre of the pluton, but have scattered abundances in the mafic rocks

(diorite and granodiorite) caused by 'mixing' between mafic phases and plagioclase, and trapped fractionated melt (Wyborn, 1983). Plots in Fig. 2 show the behaviour of Ba and Zr in whole-rock samples with respect to SiO_2, indicating by the downward inflection in element abundance the onset of crystallization of biotite (containing up to ~6000 ppm Ba) and zircon, respectively, as fractionating phases. Hafnium exhibits the same trend as Zr, but the Zr/Hf ratio decreases with fractionation possibly because of the greater relative compatibility of Zr in clinopyroxene. Yttrium abundances increase in the mafic rocks up to ~20 ppm, but jump to ~27 ppm in the outer adamellite (BP22) and then decrease into the aplite (Fig. 2). These trends reflect the increasing occurrence of interstitial Y-bearing hornblende in the mafic rocks, and its earlier (and higher-temperature) crystallization as a fractionating phase in the adamellite. Other phases contribute to these Y trends (accessory phases, K-feldspar) but hornblende is the host for ⩾60% of the whole-rock Y budget in most samples, on the basis of electron microprobe analyses and mass balance.

The REE patterns for the six whole-rock samples of this study (Fig. 3) reveal a general increase in the REE from mafic to felsic samples. This trend is reversed for BP11 (inner adamellite) and BP42 (aplite), probably because of fractionation of REE-enriched hornblende and accessory minerals. These two samples also have heavy REE (HREE) patterns that show enrichment from Gd to Lu in contrast to the mafic samples. This HREE enrichment is probably related to late-stage hydrothermal activity by the REE-rich aqueous fluid also responsible for deposition of the HREE mineral yttrobetafite. The Eu anomaly changes systematically from slightly positive in BP39 (diorite) to increasingly more negative in felsic samples, consistent with progressive removal of Eu from the crystallizing magma by feldspar fractionation.

Magma differentiation in the BPZP

Wyborn (1983) explained chemical variation within the BPZP by fractional crystallization as the main process. The following is a summary of the conclusions of Wyborn (1983).

All rocks from the BPZP are considered to be cumulates. Early crystallization was from an initially homogeneous magma with a composition of ~60 wt % SiO_2 and an intrusion temperature of ~1050°C (Wyborn, 1983; Wyborn & Chappell, 2000). This parent magma was probably crystal poor and intruded with little assimilation of country rock. Crystallization proceeded by side-wall precipitation of two pyroxenes, plagioclase and minor olivine, producing wall rocks of ~50 wt % SiO_2 and a residual melt of ~70 wt % SiO_2. This less dense residual melt was able to escape up the walls of the magma chamber by boundary-layer flow (Sparks *et al.*, 1984; McBirney *et al.*, 1985; Maaløe & McBirney, 1997). During buoyant ascent some mixing with the parent magma occurred. The main cause of differentiation of the parent magma was mixing with the ascending residual melt.

The mixing process was probably different during crystallization of the adamellite zone because the fractionated residual melt no longer had a strong density contrast with the bulk magma. In this situation mixing would have occurred locally. Such *in situ* mixing would probably have involved all of the residual melt with no residual melt ascending by boundary-layer flow. The aplite would, therefore, have crystallized from the last of the fractionated magma, not a separated residual melt.

Superimposed on whole-rock chemical trends relating to the fractionation process are processes such as flow-sorting. Field evidence and thin-section inspection show that flow-sorting involved the partial separation of pyroxene and less dense plagioclase crystals in the diorite and granodiorite zones. Sample BP16 (inner granodiorite) contains 48 ± 2% plagioclase, an amount well above that expected by the fractionation trend established in the diorite and outer granodiorite zones. Another important process was the trapping of interstitial melt, which has been shown to produce scatter and variation in whole-rock chemical trends (O'Hara & Fry, 1996*a*, 1996*b*). Although it is difficult to estimate or model the amount of trapped residual liquid (e.g. Meurer & Boudreau, 1998), from major mineral orientations and packing in the BPZP it is estimated that ~15% of the diorite zone and up to 70% of the adamellite zone consists of crystallized interstitial melt. A further process was assimilation of wall-rock. This was a very minor process producing little chemical change in BPZP magmas. The amount and nature of the assimilant is discussed in a following section. Evidence from volcanic rocks believed to be comagmatic with the BPZP indicates that apart from before crystallization of the diorite, the BPZP magma chamber did not experience pressure increase as a result of replenishment by new magma batches.

The BPZP was chosen for this study because it represents an excellent example of a zoned pluton where different rock types are essentially related to each other by simple fractional crystallization. The mineralogical and chemical characteristics of each selected whole-rock sample have been investigated, and the petrographic occurrences of zircon, apatite, titanite and other accessory phases are well constrained.

ANALYTICAL TECHNIQUES

Zircon, apatite and titanite crystals were separated from whole-rock samples by standard crushing, and heavy-liquid and magnetic separation techniques. The separated

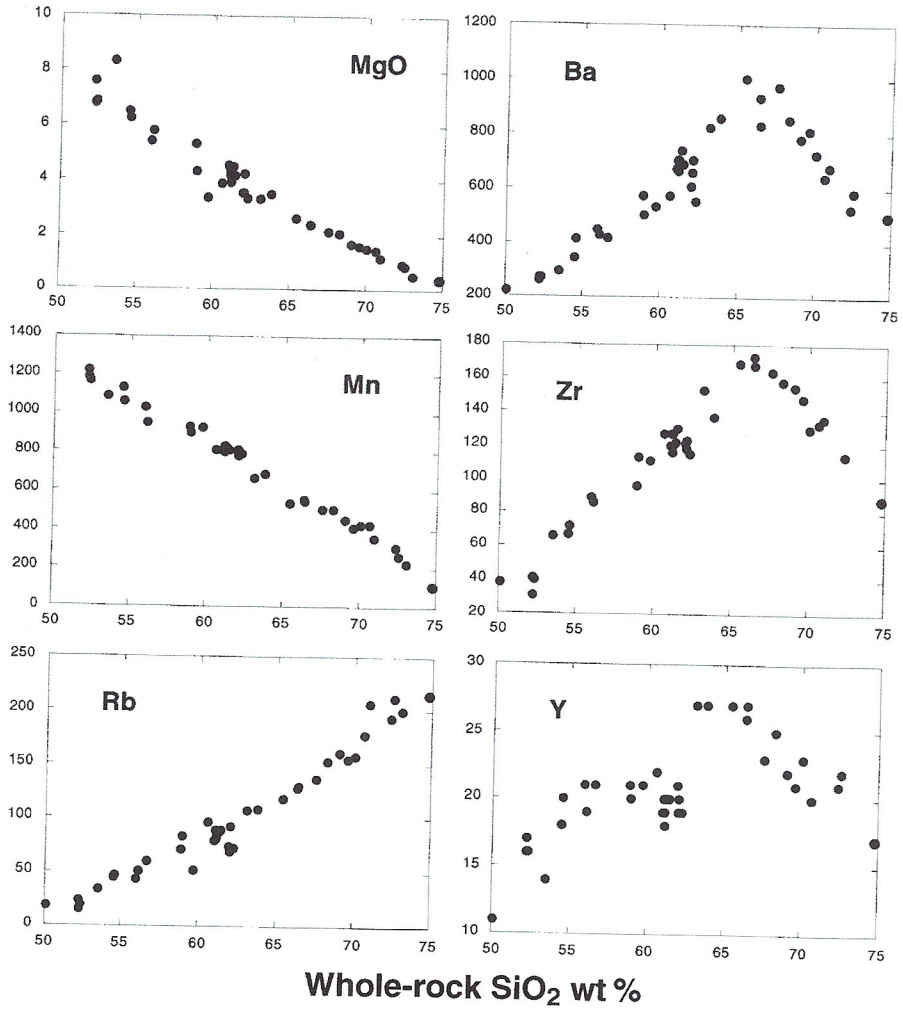


Fig. 2. Element (ppm) vs SiO_2 (wt %) plots for whole-rock samples from the Boggy Plain zoned pluton (MgO data are presented as wt % oxide). Data from Wyborn (1983).

crystals were mounted in epoxy-resin along with zircon U–Pb isotope (*SL13*) and trace element (NIST SRM 610) reference materials, sectioned and polished parallel to the longest crystal face. The same sample mounts were used for all analytical techniques (isotope and trace element analysis and CL imaging). CL imaging was performed using a Hitachi S-2250N scanning electron microscope. Uranium and Pb isotope analyses were made by secondary ion mass spectrometry (SIMS) on both the SHRIMP I and SHRIMP II ion microprobes at the Australian National University, Canberra, using the techniques of Compston *et al.* (1984) and data reduction protocols of Claoué-Long *et al.* (1995) and Williams (1998). Minor and trace element analyses were performed both by SIMS (SHRIMP I) and laser ablation (LA) inductively coupled plasma mass spectrometry (ICP-MS) according to the methods described in detail by Maas *et al.* (1992) and Hoskin (1998). Full details of analytical protocol, accuracy, precision, standardization and data reduction are provided on the *Journal of Petrology* Web site, at http://www.petrology.oupjournals.org.

RESULTS

Zircon U–Pb age of the BPZP and discussion

Uranium and Pb isotopic analysis of BPZP zircons was performed to determine the ages of inherited cores and the age of the pluton, and to test for age differences between compositional zones, within the resolution of the SIMS age determination technique. The ages of

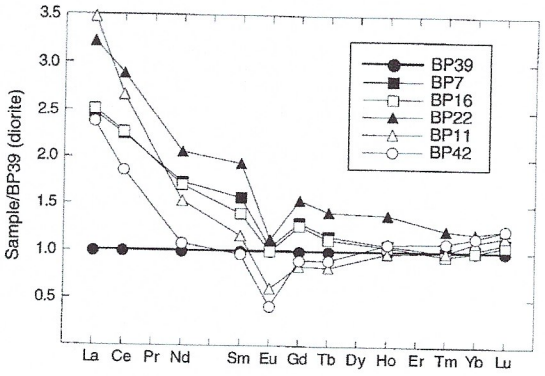


Fig. 3. Normalized REE patterns for selected whole-rock samples from the Boggy Plain zoned pluton. The samples are normalized to the most mafic sample, BP39 diorite, to magnify differences between samples. BP39, diorite; BP7, outer granodiorite; BP16, inner granodiorite; BP22, outer adamellite; BP11, inner granodiorite; BP42, aplite. Data from Wyborn (1983), analysis by INAA.

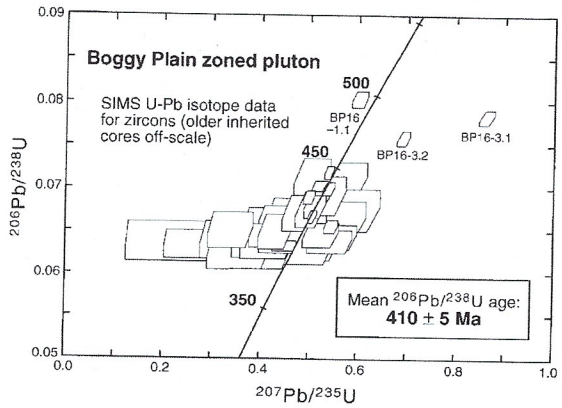


Fig. 4. Concordia diagram for U–Pb isotope analyses of Boggy Plain zoned pluton zircon. The mean age of multiple analyses on crystals from all six whole-rock samples is 410 ± 5 Ma (95% confidence level).

hydrothermal zircon rims on BP42 (aplite) zircon were also determined and the results have been presented elsewhere (Hoskin *et al.*, 1998). Multiple analyses of zircon populations separated from each of the six whole-rock samples were performed (Table 2). A majority of analyses plot on or near the concordia (Fig. 3), yielding a mean $^{206}Pb/^{238}U$ age of 410 ± 5 Ma (95% confidence level; $n = 34$; $\chi^2 = 1{\cdot}35$). This age is derived from data from all six samples, but excludes clearly discordant analyses and data from inherited cores. The age was determined using the data treatment protocols of Claoué-Long *et al.* (1995) and Williams (1998). The age is consistent with a biotite Rb–Sr age of 406 ± 5 Ma determined for a sample from the adamellite zone (Owen & Wyborn, 1979) and a number of other Rb–Sr and K–Ar ages determined for other rocks within the Boggy Plain Supersuite, which cluster about 400 Ma (Wyborn *et al.*, 1987, table 1). There are no discernible age differences between different zones of the pluton.

Ages determined for analyses on CL-imaged cores in BP16 (inner granodiorite) and BP11 (inner adamellite) confirm that the cores derive from older, inherited crystals with $^{206}Pb/^{238}U$ ages of 498, 1015, 1550, 1579 and 2647 Ma. Discordant analyses for other crystals from BP16 (inner granodiorite) suggest the presence of a component of old Pb in those crystals as well. The ages determined here fall within the ranges typically found for inherited zircon in S-type granites within the Lachlan Fold Belt (Williams, 1998) and related rocks of the Western Province, South Island, New Zealand (Muir *et al.*, 1996; Ireland & Gibson, 1998). The occurrence of these xenocrystic zircons in parts of the I-type BPZP may represent unmelted material from the magma source region or assimilation of sediments from the surrounding country rock. The scarcity of inheritance compared with S-type granitoids and its presence in only certain zones of the BPZP suggests that assimilation is the more likely source of these xenocrysts. If so, the amount of assimilation must have been very small, as whole-rock chemical relationships do not require an assimilant to explain the observed trends. Minor assimilation may have taken place at the roof of the magma chamber, where a double-diffusive layer is believed to have existed (Wyborn, 1983), and where dissolution of the assimilant might not be preserved in the chemistry of outcropping plutonic samples because of eruption of the less dense contaminated magma. Melting and mixing of the assimilant will, however, liberate accessory phases, the largest of which may sink as a result of density contrast with the surrounding melt (Bea, 1996). In this way, assimilated zircon may have been included in the crystallizing magma. The absence of zircon xenocrysts in mafic zones of the BPZP (diorite and outer granodiorite) is probably due to a higher temperature and greater degree of zircon undersaturation of the parent magma at earlier stages of crystallization. Chappell (1996) supports the process of sediment assimilation by the Boggy Plain magmas, suggesting that the slightly increasing trend in initial $^{87}Sr/^{86}Sr$ from diorite (0·70441), through adamellite (0·70479) to aplite (0·70554 in one sample) indicates minor assimilation.

Zircon chemistry

Zircon from all rock samples was analysed by LA–ICP-MS and SIMS. Results (in ppm) are presented in the Appendix (Table A1), where crystals analysed by LA–ICP-MS are labelled with a number and those analysed by SIMS with a letter. All zircons exhibit very similar chondrite-normalized REE patterns (Fig. 5), having a steeply increasing pattern over about five orders of magnitude, with strong HREE enrichment, and a positive

*Table 2: ^{204}Pb-corrected U–Pb SIMS isotope data for zircons from the Boggy Plain zoned pluton, NSW, Australia**

Grain. spot	Type	U (ppm)	Th/U	Pb (ppm)	*f* %†	$^{206}Pb/^{238}U$‡	±1σ	$^{207}Pb/^{235}U$‡	±1σ	Age§ (±1σ) (Ma)
Sample: BP42 (central aplite)										
1.1	interior	148	0·89	11	0·39	0·0642	0·0015	0·547	0·053	401 (9)
2.1	interior	210	0·71	15	0·87	0·0652	0·0014	0·478	0·038	407 (8)
3.1	interior	113	0·87	9	4·12	0·0634	0·0017	0·287	0·084	396 (10)
3.4	interior	117	0·81	9	1·83	0·0658	0·0017	0·455	0·076	411 (10)
4.3	interior	337	0·66	27	3·31	0·0637	0·0013	0·544	0·047	398 (8)
2.2	rim	1018	0·74	72	0·19	0·0635	0·0012	0·477	0·013	397 (7)
3.2	rim	3372	0·34	250	2·28	0·0683	0·0012	0·513	0·015	426 (7)
3.3	rim	6010	0·25	346	0·46	0·0584	0·0010	0·432	0·009	366 (6)
4.1	rim	10742	0·07	815	3·92	0·0711	0·0013	0·543	0·014	443 (8)
6.1	rim	4757	0·62	410	0·02	0·0803	0·0014	0·648	0·012	498 (9)
Sample: BP11 (inner adamellite)										
4.1	core	84	0·83	27	0·31	0·2717	0·0062	3·763	0·124	1550 (32)
1.2	interior	117	0·79	8	2·23	0·0620	0·0015	0·354	0·062	388 (9)
1.3	interior	112	0·76	8	1·14	0·0642	0·0016	0·482	0·047	401 (10)
3.1	interior	155	0·64	11	1·28	0·0664	0·0015	0·444	0·046	414 (9)
5.1	interior	215	0·65	15	1·12	0·0644	0·0014	0·418	0·040	402 (8)
6.1	interior	147	0·89	11	2·07	0·0633	0·0015	0·398	0·055	396 (9)
7.1	interior	147	0·86	11	0·27	0·0645	0·0015	0·525	0·037	403 (9)
1.1	rim	4929	0·29	399	7·64	0·0630	0·0011	0·504	0·021	394 (7)
Sample: BP22 (outer adamellite)										
1.1	interior	152	1·12	12	1·38	0·0632	0·0022	0·479	0·075	395 (13)
2.2	interior	151	0·95	12	2·77	0·0639	0·0022	0·347	0·070	399 (13)
2.3	interior	124	0·67	9	1·86	0·0651	0·0023	0·469	0·068	407 (14)
3.1	interior	114	0·74	9	0·83	0·0674	0·0024	0·559	0·088	420 (15)
4.1	interior	169	0·86	14	0·56	0·0706	0·0024	0·569	0·050	440 (14)
5.1	interior	128	0·73	10	4·72	0·0637	0·0024	0·229	0·103	398 (14)
6.1	interior	203	0·51	14	1·15	0·0639	0·0022	0·417	0·056	399 (13)
7.1	interior	227	0·19	15	0·88	0·0691	0·0023	0·526	0·050	430 (14)
2.1	rim	8737	0·09	613	0·71	0·0732	0·0022	0·556	0·018	455 (14)
Sample: BP16 (inner granodiorite)										
1.1	core	229	0·76	21	0·43	0·0803	0·0009	0·603	0·016	498 (6)
2.1	core	120	0·29	21	0·18	0·1706	0·0021	1·684	0·033	1015 (11)
5.1	core	124	0·72	39	0·10	0·2775	0·0032	3·765	0·057	1579 (16)
6.1	core	386	0·76	236	0·05	0·5077	0·0055	12·946	0·145	2647 (23)
3.1¶		605	0·43	55	1·35	0·0783	0·0009	0·861	0·017	486 (5)
3.2¶		655	0·50	53	1·21	0·0758	0·0008	0·693	0·014	471 (5)
4.2¶		290	2·44	20	3·85	0·0449	0·0006	0·894	0·027	283 (3)
6.3¶		170	0·62	16	3·58	0·0648	0·0008	1·301	0·045	405 (5)
1.2	interior	282	0·57	21	0·34	0·0685	0·0008	0·513	0·014	427 (5)
2.2	interior	337	0·13	22	0·10	0·0699	0·0008	0·540	0·013	435 (5)
2.3	interior	345	0·59	24	0·70	0·0655	0·0008	0·546	0·015	409 (5)
4.1	interior	264	0·60	20	0·49	0·0689	0·0008	0·502	0·012	430 (5)
5.2	interior	440	0·17	30	0·17	0·0718	0·0008	0·541	0·010	447 (5)
6.2	interior	463	0·16	29	0·15	0·0667	0·0007	0·507	0·010	416 (4)

Table 2: continued

Grain. spot	Type	U (ppm)	Th/U	Pb (ppm)	*f* %†	$^{206}Pb/^{238}U$‡	±1σ	$^{207}Pb/^{235}U$‡	±1σ	Age§ (±1σ) (Ma)
Sample: BP7 (outer granodiorite)										
1.1	interior	277	1·00	22	2·21	0·0655	0·0022	0·416	0·053	409 (13)
2.1	interior	455	1·00	36	1·77	0·0648	0·0021	0·433	0·036	405 (13)
3.1	interior	323	0·55	23	1·59	0·0644	0·0021	0·443	0·045	402 (13)
4.1	interior	354	0·95	28	3·11	0·0650	0·0021	0·340	0·047	406 (13)
5.1	interior	390	0·52	28	1·03	0·0670	0·0022	0·479	0·034	418 (13)
6.1	interior	312	0·57	23	1·79	0·0666	0·0022	0·462	0·050	416 (13)
7.1	interior	1028	1·52	93	0·44	0·0686	0·0021	0·512	0·022	428 (13)
Sample: BP39 (diorite)										
1.1	interior	109	0·54	8	1·99	0·0638	0·0023	0·485	0·083	399 (14)
2.1	interior	252	0·83	21	1·00	0·0712	0·0023	0·507	0·039	443 (14)
3.1	interior	175	0·64	13	3·25	0·0636	0·0022	0·362	0·065	397 (13)
4.1	interior	140	0·65	10	1·63	0·0661	0·0023	0·533	0·084	412 (14)
5.1	interior	515	1·00	41	0·56	0·0675	0·0021	0·504	0·032	421 (13)
6.1	interior	249	0·93	19	1·14	0·0647	0·0021	0·468	0·042	404 (13)
7.1	interior	167	0·68	12	2·53	0·0626	0·0021	0·401	0·065	392 (13)

*Data for all samples except BP16 were collected in 1990 on SHRIMP I; BP16 was analysed in 1997 on SHRIMP II.
†Refers to the percentage of measured ^{206}Pb that is non-radiogenic; estimated from the measured $^{204}Pb/^{206}Pb$ ratio and assuming 400-My-old common Pb (Stacey & Kramers, 1975).
‡Ratios refer to radiogenic Pb. Pb/U ratios were normalized by concurrent analyses of the reference zircon *SL13* where $^{206}Pb/^{238}U = 0·0928$.
§$^{206}Pb/^{238}U$ age.
¶Discordant analysis; contribution from old Pb.

Ce and negative Eu anomaly. Chondrite normalizing values in this paper are those of McDonough & Sun (1995). This style of zircon REE pattern is that typically reported for igneous zircon analysed *in situ* by a microprobe technique (Barbey *et al.*, 1995; Bea, 1996). Within a single population there can be more than an order of magnitude variation in individual REE abundances, although the shape and slope of individual patterns do not change significantly. The REE abundance range measured for each population significantly overlaps all other populations (Fig. 6) revealing no systematic changes in zircon REE patterns from whole-rock samples spanning the margin to the centre of the pluton. However, there is an apparent trend between samples in the lowest measured REE abundance of each zircon population. Plots of Y and Yb (Fig. 7) reveal an increase in the lower limit of each abundance range for zircon populations from mafic whole-rock samples (diorite, granodiorite), and a decrease in felsic samples (adamellite, aplite). Except for Ce, which broadly increases in abundance from mafic to felsic, all zircon REE heavier than Pr exhibit this trend, which mimics the measured trend in whole-rock samples (Fig. 2), where Y abundances (a proxy for the HREE) increase in mafic zones and decrease in felsic zones.

The size of the Ce anomaly in all zircon REE patterns does not vary systematically between samples despite a broad increase in Ce abundance from mafic to felsic, with values of Ce/Ce^* [equal to $Ce_N/(La_N \times Pr_N)^{0·5}$] averaging ~38. Values of the Eu anomaly in zircon decrease in the mafic rocks (Fig. 7) although there is considerable range in Eu/Eu^* within each population. The decrease in Eu/Eu^* cannot be caused by decreasing melt fO_2 in which the Eu^{2+}/Eu^{3+} ratio is increasing, but is consistent with growth from a melt that has experienced plagioclase fractionation and is, therefore, depleted in Eu. The jump in Eu/Eu^* values for zircon from felsic zones (adamellite, aplite) probably represents zircon saturation and crystallization in the bulk melt at this stage of differentiation (BP22, outer adamellite).

Thirteen other trace elements were analysed in zircon by LA–ICP-MS. In analyses where the abundances of the REE are high, other trace element abundances are also high. There is a sympathetic relationship between Y + REE and P, suggesting the 'xenotime' substitution

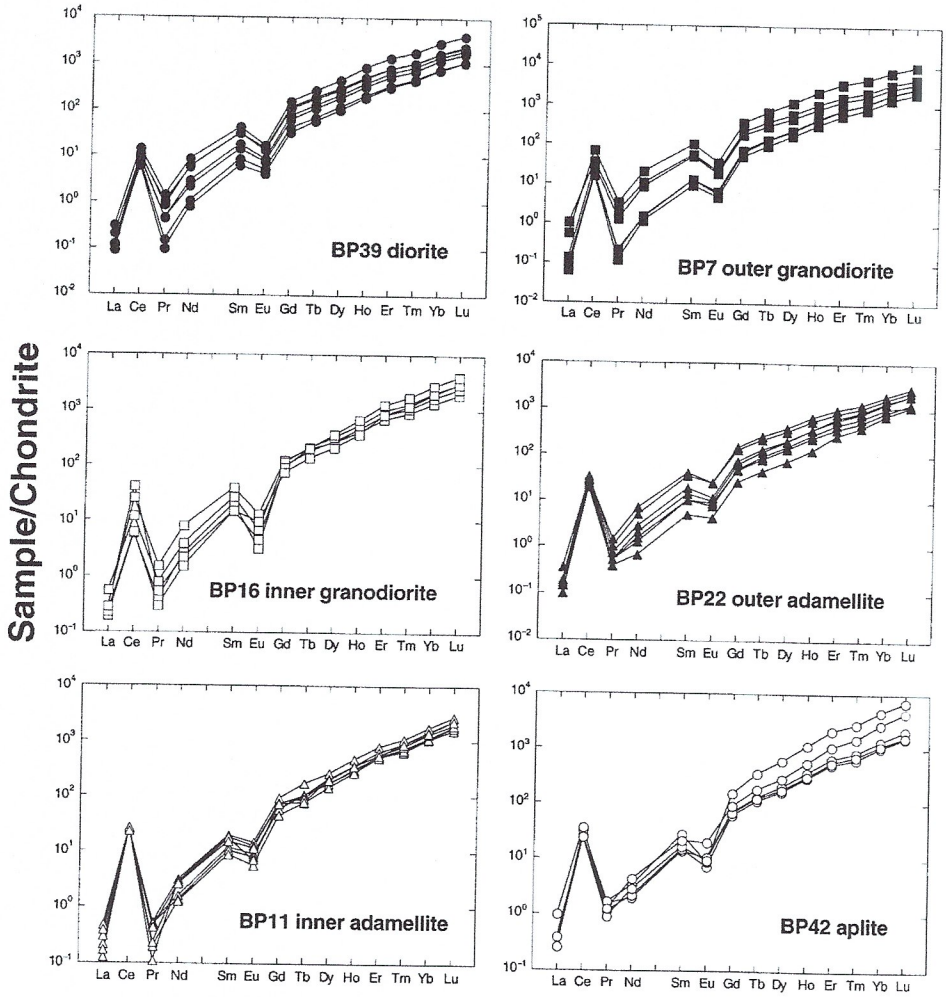


Fig. 5. Chondrite-normalized REE diagrams for zircon from the Boggy Plain zoned pluton. Data from SIMS analyses.

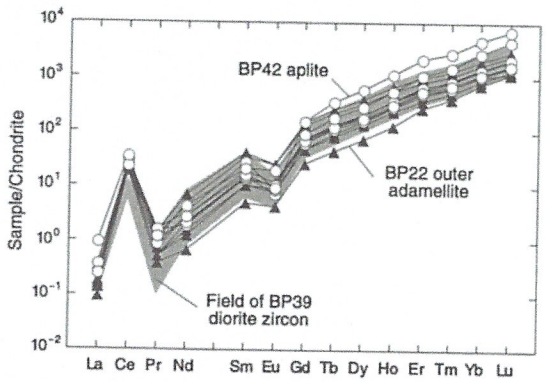


Fig. 6. Chondrite-normalized REE diagrams for selected zircon populations from the Boggy Plain zoned pluton.

mechanism is partially responsible for charge balance of trace element 'impurities'. There are broad increases in the abundances of P (Fig. 7), Ca, Sc, Nb, Hf (see also SIMS data) and Ta from mafic to felsic zones, but there are large abundance ranges within each population. The abundances of Th and U are those typically observed in igneous zircon, with the Th/U ratio ranging from 0·6 to 1·2, averaging ~0·9. The abundance ranges of Th and U are much smaller in felsic zones relative to mafic zones, with maximum abundances not exceeding ~350 ppm and ~470 ppm, respectively, whereas in mafic zones, zircon Th and U abundances may exceed 1000 ppm. The restriction of zircon Th and U abundances in felsic zones is possibly due to the co-crystallization of other Th- and U-bearing phases, allanite and monazite in particular (Table 1).

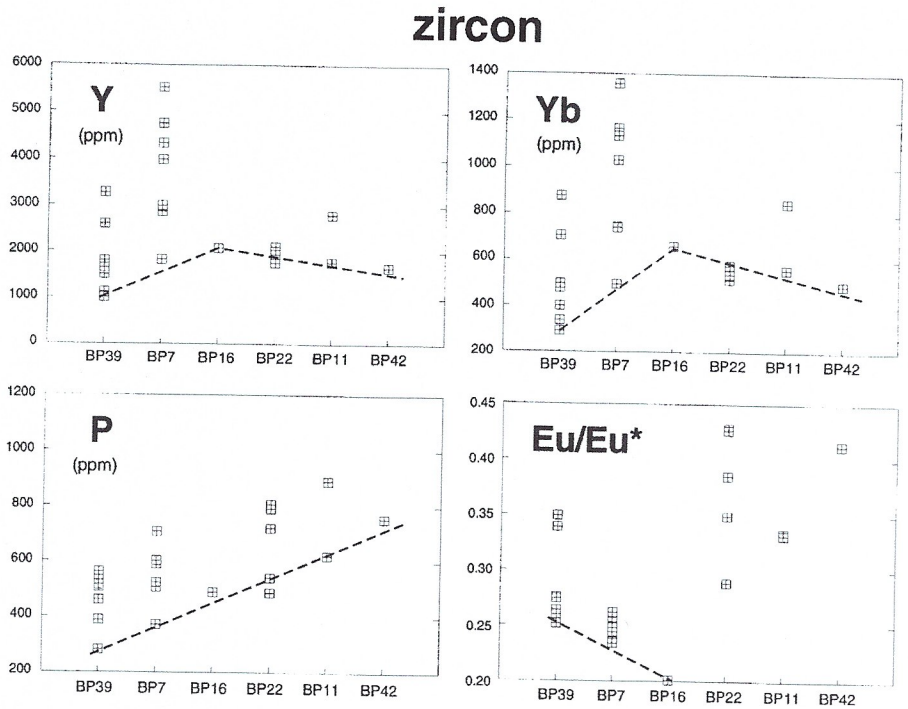


Fig. 7. Selected plots revealing chemical trends between zircon populations from most mafic to more felsic whole-rock samples from the Boggy Plain zoned pluton. Data from LA–ICP-MS analyses. BP39, diorite; BP7, outer granodiorite; BP16, inner granodiorite; BP22, outer adamellite; BP11, inner adamellite; BP42, aplite. On each plot whole-rock composition changes from most mafic to most felsic from left to right.

Apatite chemistry

Tabular euhedral apatite from all rock samples was analysed by LA–ICP-MS (Appendix, Table A2) and by electron microprobe (EMP). EMP analyses show that the apatites have relatively uniform abundances of F from the margin to the centre of the pluton, with population averages ranging from 1·9 to 2·7 wt %. Chlorine abundances in apatite from mafic zones (diorite, granodiorite) are relatively high (averages ranging from 0·36 to 0·57 wt % Cl), but are low in felsic zones (adamellite, aplite; averages ranging from 0·05 to 0·09 wt % Cl) where OH abundances are higher. There are no systematic increases in F or Cl abundances with fractionation. Manganese abundances in apatite measured by EMP increase systematically from 0·018 wt % Mn in the diorite to 0·08 wt % Mn in the aplite. Apatite from BP16 (inner granodiorite) does not fit this trend and is anomalously enriched in Mn.

The normalized REE plots for BPZP apatite populations (Fig. 8), like those for zircon, are similar between samples. The patterns decrease steeply from the LREE (i.e. La–Sm) to the HREE over about two orders of magnitude, and have prominent negative Eu anomalies. Despite general similarity the patterns do differ between samples (Fig. 9). In mafic zones there is a relatively large abundance range for each apatite population, whereas in felsic zones there is remarkable homogeneity and the REE patterns within any one population are tightly clustered. This may indicate saturation of apatite in the bulk magma at the granodiorite–adamellite boundary, where previously in more mafic zones apatite growth occurred in trapped intercumulus liquids having divergent and scattered REE abundances.

The slope of the LREEs becomes steeper (i.e. Sm_N/La_N decreases) in mafic zones as differentiation proceeds (Fig. 10), but remains approximately constant in felsic zones. The value of Sm_N/La_N for apatite in felsic zones is higher on average than in the granodiorite, such that the flatter LREE patterns in the adamellite and aplite probably reflect depletion of the melt by an LREE-rich phase, probably allanite. This is also indicated by a change in the shape of the LREE pattern from straight in granodiorite apatite to curved in adamellite and aplite apatite indicating, in particular, removal of La, Ce and Pr from the melt (the apparent LREE curvature in BP39 diorite apatite is due to overlapping curves). The occurrence of euhedral allanite at the granodiorite–adamellite boundary (Table 1) coincides with the change from increasing La, Ce and Pr abundances in diorite and granodiorite apatite to more uniform abundances in

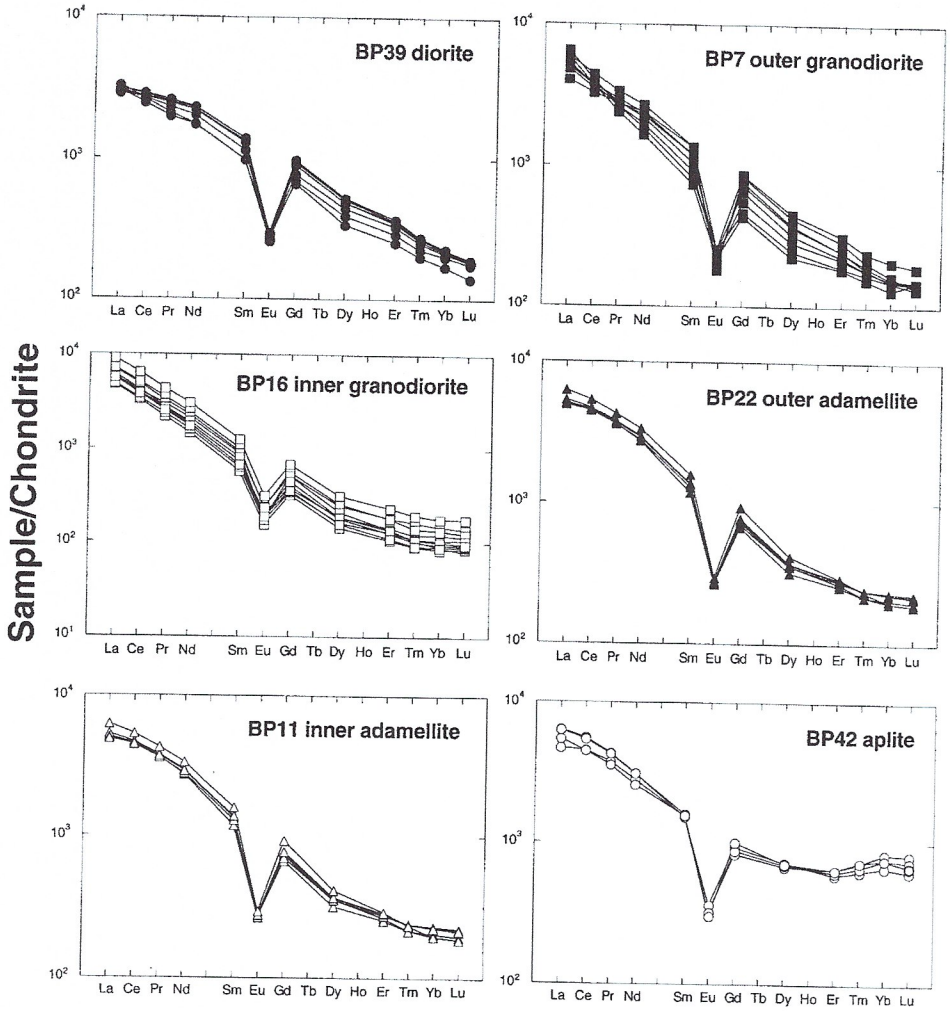


Fig. 8. Chondrite-normalized REE diagrams for apatite from the Boggy Plain zoned pluton. Data from LA–ICP-MS analyses.

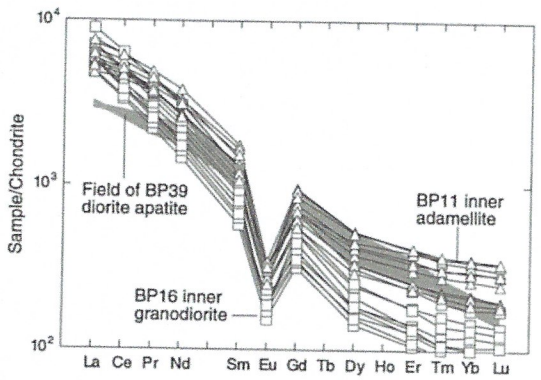


Fig. 9. Chondrite-normalized REE diagrams for selected apatite populations from the Boggy Plain zoned pluton.

apatite from felsic zones. The curvature in the HREE patterns for all apatites except BP39 (diorite) may reflect melt depletion by clinopyroxene, hornblende and possibly zircon. The abundances of Y (Fig. 10), Nd, Sm, Eu and the HREE in apatite decrease in mafic zones, but increase in felsic zones (the HREE enrichment in BP42, aplite, is considered anomalous and to be related to hydrothermal alteration). These trends are opposite to those observed in the whole rock (Fig. 2) and in zircon (Fig. 7). Values of Eu/Eu* in apatite are in the range 0·17–0·40 and are similar in all samples from pluton margin to centre, averaging 0·30.

Apatite from sample BP39 (diorite) contains ~530 ppm Sr, which decreases in abundance from mafic to felsic zones (Fig. 10). This decreasing trend for Sr is also observed for feldspar (Wyborn, 1983), so that the decrease in apatite Sr probably reflects the depletion of Sr from

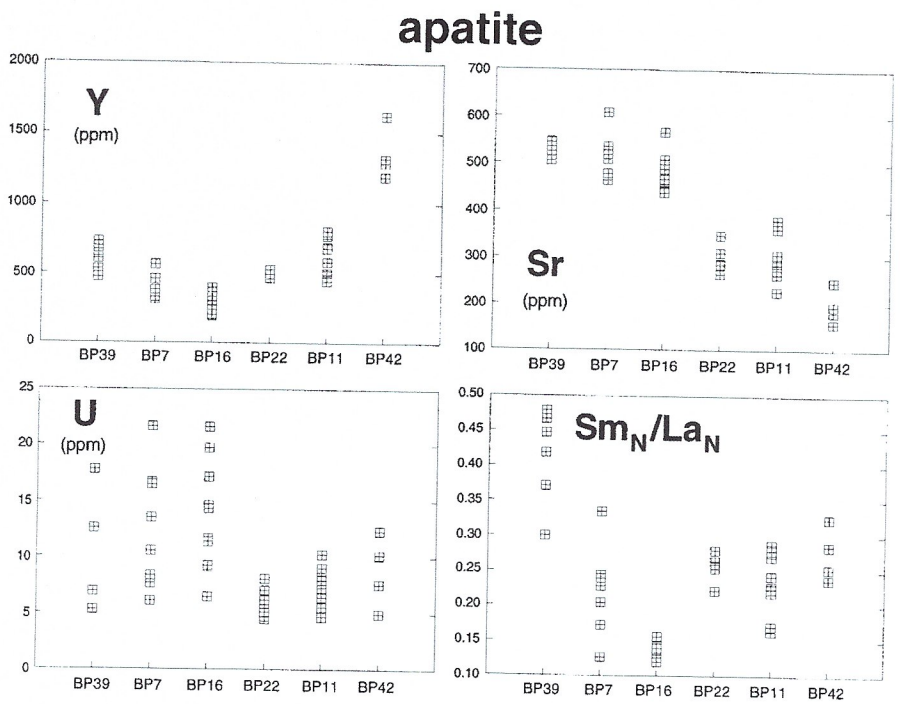


Fig. 10. Selected plots revealing chemical trends between apatite populations from most mafic to more felsic whole-rock samples from the Boggy Plain zoned pluton. BP39, diorite; BP7, outer granodiorite; BP16, inner granodiorite; BP22, outer adamellite; BP11, inner adamellite; BP42, aplite. On each plot whole-rock composition changes from most mafic to most felsic from left to right. The subscript 'N' denotes that the abundance value is chondrite normalized.

the melt by feldspar crystallization. Average abundances of Th and U in apatite are also lower in felsic zones (Fig. 10), and, as for zircon, this probably reflects the co-crystallization of allanite and possibly monazite. Lithium, Ba and Hf exhibit general enrichment trends in apatite from mafic to felsic zones. Silicon abundances vary widely within an apatite population but sympathetically with Y + REE abundances, indicating element substitution by the following mechanism: $(Y, REE)^{3+} + Si^{4+} = Ca^{2+} + P^{5+}$. Sodium abundances were not determined for these apatites, but element substitution coupled with Na is likely: $REE^{3+} + Na^{+} = 2Ca^{2+}$ (Rønsbo, 1989).

Titanite chemistry

Within the BPZP, titanite occurs in the granodiorite and adamellite as a primary magmatic phase (Table 1). Titanite from the inner granodiorite (BP16) and adamellite (BP22, BP11) zones was analysed by LA–ICP-MS (Appendix, Table A3) and EMP. The abundances of Al_2O_3 and Fe_2O_3 increase from the inner granodiorite (1·11 and 1·22 wt %, respectively) to the adamellite zone, where abundances are relatively uniform (1·18 wt % Al_2O_3 and 1·86–1·91 wt % Fe_2O_3).

The normalized REE patterns for titanite differ significantly between samples (Figs 11 and 12). Titanite from sample BP16 (inner granodiorite) is LREE enriched relative to the HREE, which have a flatter normalized slope. The Eu anomaly varies from positive to negative. In the adamellite zone, titanite REE patterns from both the inner and outer adamellite have similar shaped patterns showing weak LREE enrichment, nearly flat HREE abundances, and a negative Eu anomaly. Abundances for individual REE within a population can range over half an order of magnitude. As differentiation proceeds, the titanite REE pattern progressively becomes flatter as the Lu_N/Ce_N ratio increases as a result of relatively lower abundances of the LREE (Fig. 13). The shape of the LREE pattern also changes progressively, with a stronger downward curvature in more felsic samples because of relatively decreasing abundances of La, Ce and Pr. Lanthanum, in particular, becomes strongly depleted, resulting in decreasing values of La_N/Ce_N (Fig. 13) from the granodiorite to the inner adamellite. The relative decrease in LREE abundances with differentiation probably reflects apatite and allanite fractionation, with allanite strongly influencing the abundances of La and Ce (and La_N/Ce_N) in the melt.

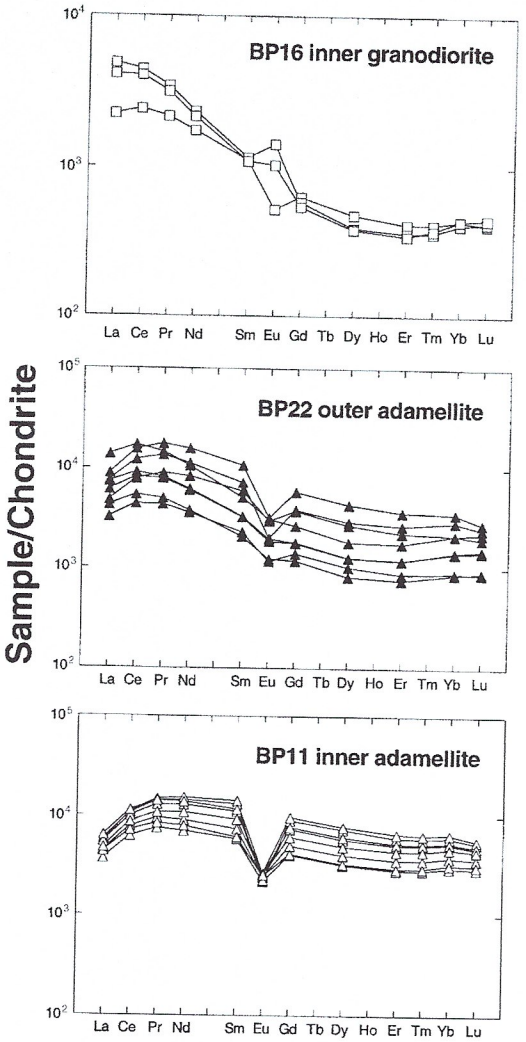


Fig. 11. Chondrite-normalized REE diagrams for titanite from the Boggy Plain zoned pluton. Data from LA–ICP-MS analyses.

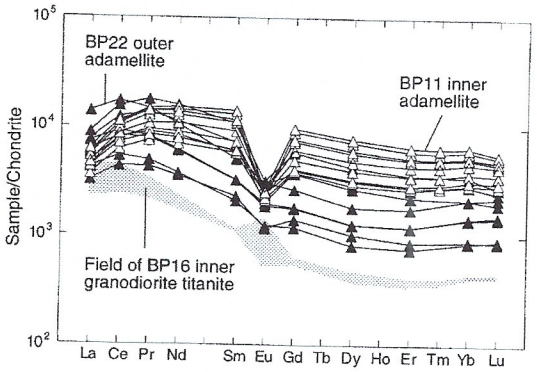


Fig. 12. Chondrite-normalized REE diagrams for selected titanite populations from the Boggy Plain zoned pluton.

Positive Eu anomalies (Eu/Eu* >1) have been observed in titanite from intermediate composition granitoids elsewhere in the Lachlan Fold Belt (Bingie Bingie Point) and intermediate composition volcanics, Eastern Pontides, Turkey (P.W.O. Hoskin, unpublished data, 2000). Titanite in granodiorite from the McMurry Meadows Pluton, CA, USA, has no Eu anomaly (Sawka, 1988), a feature that has also been reported by Bea (1996) as typical for titanite from metaluminous and peralkaline granitoids analysed in that study. Titanite in the inner granodiorite from the BPZP has values of Eu/Eu* ranging from 0·62 to 1·74. This ratio progressively decreases in more felsic samples (Fig. 13) to values ranging from 0·20 to 0·45 in the inner adamellite. This decreasing Eu/Eu* trend is not observed in zircon from the same samples (Fig. 7), but if the euhedral zircon in these rocks crystallized early, then the trend observed in titanite can be explained by late crystallization of titanite, which is interstitial in these rocks (Table 1), after significant crystallization of feldspar.

Despite increasing Lu_N/Ce_N values and a flatter normalized REE pattern for titanite as differentiation proceeds, the absolute abundances of all REE and Y (Fig. 13) broadly increase from the inner granodiorite to the inner adamellite. This trend is similarly observed for apatite (Fig. 10), but not for zircon (Fig. 7). The average sum of Y + REE (ΣREE) rises from ~5500 ppm in titanite from the inner granodiorite to ~26 000 ppm in titanite from BP11 (outer adamellite). Manganese, Zr, Nb, Hf, Ta and U also exhibit broad increases in abundance from mafic to felsic samples, whereas Sr and V (Fig. 13) decrease. Scandium is most enriched in titanite from BP11 (inner adamellite). The increasing abundances of ΣREE and Fe_2O_3 (and uniform Al_2O_3) in titanite suggest that element substitution is occurring by the following mechanisms: $(Y, REE)^{3+} + (Fe, Al)^{3+} = Ca^{2+} + Ti^{4+}$ and $(Mn, Sr)^{2+} = Ca^{2+}$, with other mechanisms involving P^{5+} substitution in the Si^{4+} tetrahedral site, $(V, Nb, Ta)^{5+}$ in the Ti^{4+} octahedral site, and $(OH, F)^-$ in an O^{2-} site likely (Smith, 1970; Clark, 1974).

Summary of compositional changes in zircon, apatite and titanite from the BPZP

Zircons from all zones of the BPZP have HREE-enriched chondrite-normalized REE patterns that are remarkably uniform despite large abundance ranges within individual populations. There are no systematic changes in the shape of the zircon REE patterns with increasing differentiation. The negative Eu anomaly in zircon increases from diorite to granodiorite and is smaller in felsic zones. Some trace elements (P, Ca, Sc, Nb, Ce, Hf, Ta) increase in zircon from mafic to felsic zones, whereas others (Th and U)

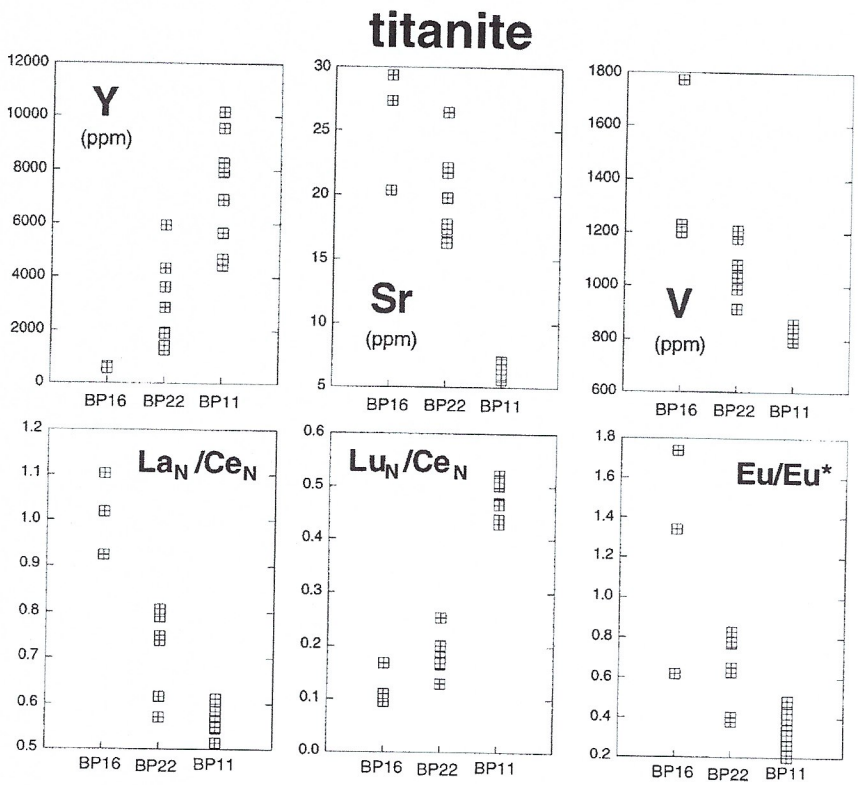


Fig. 13. Selected plots revealing chemical trends between titanite populations from more mafic to more felsic whole-rock samples from the Boggy Plain zoned pluton. BP16, inner granodiorite; BP22, outer adamellite; BP11, inner adamellite. On each plot whole-rock composition changes from more mafic to more felsic from left to right.

have more uniform, restricted abundances in felsic zones.

Chondrite-normalized apatite REE patterns are LREE enriched. REE patterns for apatite from felsic zones are tightly clustered, in contrast to patterns from mafic zones. The normalized LREE pattern is straight in apatites from mafic zones, but is concave-down in felsic zones. All apatites have a concave-up HREE pattern, except those in BP39 (diorite), for which that part of the REE pattern is straight. The abundances of the REEs heavier than Pr decrease in mafic zones with differentiation, but in apatites from felsic zones the abundances progressively increase. The abundances of Li, Mn, Ba and Hf increase in apatite from mafic to felsic zones, but Sr abundances decrease. As for zircon, the abundances of Th and U are more uniform in felsic zones relative to apatites in mafic zones.

Titanite, relative to zircon and apatite, exhibits the most pronounced changes in REE chemistry with differentiation. In the granodiorite titanite is LREE enriched, but in the adamellite the degree of LREE enrichment is lower, producing a REE pattern that is nearly flat. The relative abundances of La, Ce and Pr decrease as differentiation progresses, resulting in increasing LREE downward curvature. The Eu anomaly in titanite systematically increases from more mafic to more felsic zones. The abundances of Mn, Fe^{3+}, Y, Zr, Nb, REE, Hf, Ta and U in titanite increase with differentiation, whereas the abundances of V and Sr decrease.

DISCUSSION

Saturation points of accessory minerals in the BPZP

As discussed in the Introduction, various methods and criteria are used to identify accessory mineral saturation points within cogenetic granitoid suites. The nature of granitoid rocks as composites of melt and crystals, and the range of possible processes that can operate during melting, ascent and solidification, can make it difficult to identify saturation points with certainty using a single method or criterion.

Morphology, 'inverse' modelling and saturation calculations

Saturation and early crystallization of accessory minerals in granitoids is difficult to demonstrate on petrographic

criteria. Euhedral crystal morphologies and inclusion in major rock-forming phases are two petrographic criteria that have been used to support interpretations of early crystallization of accessory phases in plutonic rocks (e.g. Gromet & Silver, 1983; Sawka, 1988; Shannon *et al.*, 1997; Warner *et al.*, 1998). According to these criteria, within the BPZP (Table 1), apatite was always saturated and zircon almost always but not within the diorite. Allanite would have saturated at the granodiorite–adamellite boundary. Titanite is only likely to have been saturated in the aplite, where it has been hydrothermally replaced. Monazite is nowhere observed with euhedral morphology.

Crystallization of REE-rich accessory minerals in granitoid magmas is expected because these minerals are composed of essential structural constituents (ESCs) that are incompatible trace elements in major rock-forming minerals. If a volume of trapped intercumulus melt is not already saturated in a given accessory mineral, crystallization of major phases will increase accessory mineral ESC concentrations in the shrinking residual melt until saturation occurs. The crystallization of accessory minerals in this way occurs far from the liquidus of the parent magma. These far-from-liquidus accessory phases may form from the melt with euhedral crystal faces and be included in major rock-forming phases (e.g. zircon in websterite, eclogite and gabbro: Gaggero & Gazzotti, 1996; von Quadt *et al.*, 1997; Brueckner *et al.*, 1998) revealing why euhedral morphology is not a reliable criterion for identifying accessory mineral saturation points.

The 'inverse' modelling approach to recognizing accessory mineral saturation was applied by Evans & Hanson (1993) to identify zircon saturation and fractionation, based on an earlier demonstration by Hanson (1989). This approach to identifying the role of mineral phases and processes that operated within a suite of cogenetic magmas does not presuppose any particular mineral assemblage as is necessary for mass-balance process modelling (i.e. 'forward' modelling). Using element scatter plots, the 'inverse' approach can provide constraints on processes, compositions and mineralogy before 'forward' calculations are performed. Element variations as a function of whole-rock SiO_2 abundance (as an index of differentiation) for samples from the margin to the centre of the BPZP are plotted in Fig. 14. The elements selected (except Nb) are ESCs in the REE-enriched accessory phases found in BPZP whole-rock samples (Table 1). Niobium was selected instead of TiO_2 (which is strongly partitioned into biotite, possibly masking the effect of titanite saturation on whole-rock TiO_2 abundance) because it is enriched in BPZP titanite with abundances ranging up to $1{\cdot}67 \times 10^4$ times chondrite (Appendix, Table A3).

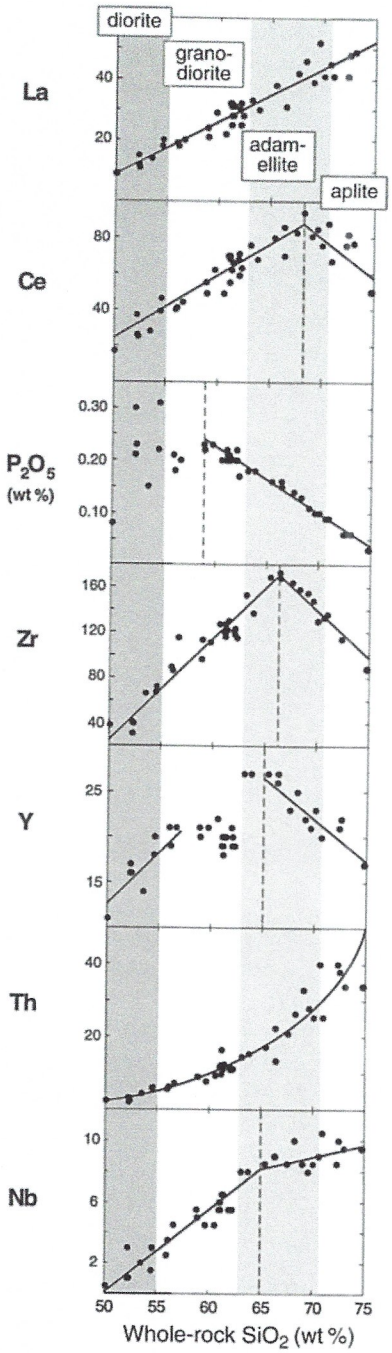


Fig. 14. Element scatter plots for whole-rock samples from the BPZP indexed against SiO_2 abundance. The continuous trend lines are fitted 'by eye'. Dashed vertical lines indicate points at which element abundance trends change in response to mineral saturation and fractionation. Element abundances are in ppm, except P_2O_5, which is in wt %. The shaded regions indicating different compositional zones from the margin to the centre of the pluton are approximate only. Data from Wyborn (1983).

Accessory mineral saturation is interpreted from ESC–SiO_2 plots to occur at the point where the ESC abundance becomes relatively uniform with increasing differentiation (Hanson & Langmuir, 1978). An implicit assumption is that the ESC is solely (or at least predominantly) contained within the accessory mineral and not within other phases. A downward inflection on an element–SiO_2 plot indicates that the element has become 'compatible' (i.e. $K_d > 1$) in a fractionating phase. However, this inflection may also occur by combined accessory mineral saturation and element compatibility in a major rock-forming phase. A further assumption is that once accessory mineral saturation is attained, that phase will fractionate from the melt. In the BPZP both La and Ce are ESCs in allanite and monazite. EMP analyses reveal that both phases are Ce rich. The inflection in Ce abundances at ~68 wt % SiO_2 (Fig. 14) is interpreted to represent allanite saturation, not monazite saturation, which would be expected to produce an inflection in La abundances as well, given its high La_2O_3 content (~16 wt %). The Ce inflection occurs ~3 wt % SiO_2 after the appearance of euhedral allanite (Table 1) near the granodiorite–adamellite boundary in BP22 (outer adamellite). This might suggest that allanite was not saturated in BP22, although it is probable that the aplite samples are slightly LREE enriched from hydrothermal alteration, and that the Ce inflection actually occurs closer to ~65 wt % SiO_2.

Allanite also contains Th as an ESC (at ~1 wt % ThO_2) as does monazite (~2 wt % ThO_2). As a result of low abundances of Th as an ESC in these phases no Th inflection is observed, but Th abundances increase with SiO_2, illustrating the effects of *in situ* fractionation (Langmuir, 1989). Apatite saturation is indicated on the P_2O_5–SiO_2 plot to occur in the granodiorite at ~59 wt % SiO_2, and zircon saturation occurs in the outer adamellite (BP22) at ~66 wt % SiO_2 as indicated on the Zr–SiO_2 plot. For both P_2O_5 and Zr, abundances decrease steeply after saturation, indicating compatibility in other phases as well as ESC saturation, and perhaps a decreasing saturation surface as melt compositions evolve and temperature falls. There is no accessory mineral in the BPZP that contains Y as a significant ESC, so the decreasing Y abundances in the adamellite and aplite from ~65 wt % SiO_2 represent Y compatibility in hornblende and biotite as indicated by increased Y abundances in these minerals (Wyborn, 1983). These major mineral phases also fractionate TiO_2, masking the potentially recorded onset of titanite saturation. Although Nb is not an ESC in titanite, its mineral–melt K_d is ~6 in intermediate and felsic melts (Green & Pearson, 1987) and measured abundances are high in BPZP titanite such that a Nb–SiO_2 plot may indicate titanite saturation. A change in Nb compatibility is observed on the Nb–SiO_2 plot at ~65 wt % SiO_2 and it is likely that this relates to compatibility changes for Y and Ba at 65 wt % SiO_2 as a result of hornblende and biotite fractionation, and not titanite fractionation; Nb occurs in biotite from the adamellite and aplite at an average abundance of 155 ppm (Wyborn, 1983), so the whole-rock budget of ~9 ppm could be accommodated by only 6 modal % biotite.

In most studies where it is of interest to know whether or not a particular accessory phase was saturated in a sample, a whole-rock chemical database for related rocks is absent and 'inverse' modelling is not possible. Experimental investigations of accessory mineral saturation do, however, provide precise methods for determining the saturation behaviour of specific phases in an individual whole-rock sample. Comprehensive studies have so far been conducted on zircon, apatite, titanite and monazite (Harrison & Watson, 1983, 1984; Watson & Harrison, 1983; Green & Pearson, 1986; Montel, 1986; Rapp & Watson, 1986), and show that saturation is a function of accessory mineral ESC concentration and melt composition. Zircon and apatite saturation models may be expressed as saturation temperatures, that is, the temperatures at which a given melt is saturated in zircon or apatite. Zircon saturation calculations (Watson & Harrison, 1983) for BPZP samples indicate that zircon saturated in the bulk magma during crystallization of the outer adamellite (sample BP22) at a temperature of ~765°C (Fig. 15), which falls within the 700–800°C range for the BPZP felsic rocks estimated from biotite–apatite geothermometry (Wyborn, 1983). The uncertainty for zircon saturation temperatures is estimated to be ~ ±5–7%. As expected, the saturation temperatures fall slightly as the magmas become more evolved. In the diorite and granodiorite zones, calculated zircon saturation temperatures (filled diamonds in Fig. 15) are lower than magma temperatures of ~900–950°C (± 40°C) estimated from two-pyroxene geothermometry (Wyborn, 1983), indicating that zircon was not an early crystallizing phase. The Watson & Harrison (1983) model is not constrained for melts with M values >1·8 [where M is the cation ratio: (Na + K + 2Ca)/(Al × Si)], so the calculated zircon saturation temperatures for the mafic BPZP rocks for which M values range from 3·02 (BP39 diorite) to 1·80 (BP16 inner granodiorite) are probably poor estimates. Better estimates can be obtained by varying the value of M in the saturation temperature calculations (open diamonds in Fig. 15) by increasing the SiO_2 abundance of the sample to 60–65 wt % SiO_2, a better estimate of the original melt composition. Euhedral granodiorite zircon and anhedral–subhedral diorite zircon crystallized from trapped intercumulus melt where 'localized saturation' for zircon was attained. A similar zircon saturation surface to the BPZP was calculated by Evans & Hanson (1993, fig. 6) for their whole-rock suite. The rising saturation temperature for zircon before it becomes saturated in the bulk magma is expected and

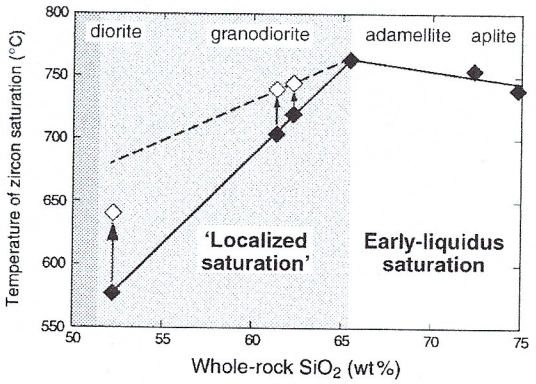


Fig. 15. Calculated zircon saturation temperatures (Watson & Harrison, 1983) indexed against the whole-rock SiO_2 abundance for samples from the BPZP. ◆, *M* values calculated from whole-rock analyses; ◇, estimated *M* values by realistic variation of SiO_2 abundances. Zircon is saturated in the felsic zones (from ~65 wt % SiO_2), but mafic zones only attain 'localized saturation' within intercumulus melt pools (shaded region).

is not an 'artefact of the differentiation process' (Sawka, 1988, p. 167).

Apatite saturation temperatures (Harrison & Watson, 1984) for BPZP samples range from 840°C to 905°C. In mafic zones of the BPZP, where zircon saturation temperatures are low, the calculated apatite saturation temperatures are in the range 870–896°C, within the uncertainty limits of the pyroxene geothermometer range of 900–950°C (±40°C). The lower temperature limit of 870°C was calculated for apatite saturation in BP39 (diorite) based on an SiO_2 abundance of 60 wt % although the whole rock—a cumulate—contains only 53 wt % SiO_2, so this temperature is considered a maximum estimate. For this reason the diorite zone was probably not saturated for apatite, as also indicated by 'inverse' modelling. Saturation temperatures of 840–905°C in BPZP felsic zones are higher than estimates from biotite–apatite geothermometry and zircon saturation temperatures, indicating that apatite was an early crystallizing phase in all of these zones. The high temperatures suggest that both the adamellite samples (BP22, BP11) and aplite sample (BP42) have a small excess component of apatite. The sample (BP22) with the 905°C calculated apatite saturation temperature could represent a magma with a temperature of 765°C (zircon saturation temperature) and only 0·29 wt % excess apatite. This may not be surprising given the relatively low density of apatite (2·9–3·5 g/cm^3), the density and viscosity of felsic melts and, therefore, the possibility that apatite crystals may not fractionate efficiently from the melt. Another explanation for the high apatite saturation temperatures calculated for BPZP felsic zones may be that it is inappropriate to apply the Harrison & Watson (1984) saturation model to these rocks, which have increasing alumina saturation and become mildly peraluminous in the inner adamellite and aplite (see Chappell, 1999). It may be more useful in this case to consider the apatite solubility models of Bea *et al.* (1992) and Wolf & London (1994), determined using natural samples and experiments on compositions more peraluminous than the felsic zones of the BPZP.

Independent experimental studies indicate that the solubility of monazite in a felsic melt can be described simply by the total amount of REE dissolved in the melt at a given temperature (Montel, 1986, 1993; Rapp & Watson, 1986). Pressure has little, if any, effect on monazite solubility, although the water content of a melt does have a minor effect. Assuming a dissolved water content of 3 wt % in Boggy Plain magmas, equation (1) of Montel (1993) indicates that the BPZP adamellite and aplite zones would have been saturated for monazite below 775°C. It does not appear, however, that the BPZP anhedral–subhedral La,Ce-monazite was an early crystallizing phase because no evidence of La depletion is preserved in whole-rock chemistry (Fig. 14). The reason why monazite did not saturate and crystallize in the bulk magma may be the stabilization of allanite over monazite as an LREE ESC-bearing phase (Cuney & Friedrich, 1987), or simply that early crystallization of allanite and apatite depleted the melt in the LREE so that monazite could not saturate until much lower temperatures. Comparison of the TiO_2 abundances of ilmenite-free BPZP mafic rocks with the abundances in experimental melts from a Ti-rich accessory-mineral saturation study (Green & Pearson, 1986) suggests that the BPZP rocks were not saturated for titanite, but that it may have been an early crystallizing phase in the aplite where the crystallization temperature of the bulk melt was lower.

Zircon, apatite and titanite trace element chemistry

It is accepted that in most intermediate–felsic magmas the behaviour and abundances of the REEs are controlled by accessory minerals. In rock suites such as that studied by Wark & Miller (1993), where accessory minerals record melt compositional changes that occurred during differentiation, it is logical to conclude that changes in the REE chemistry of a given accessory mineral across a suite are recording the effects of other accessory minerals (and even earlier crystallization of itself) on the REE characteristics of the melt. Therefore, in a general sense, the changes in accessory mineral REE characteristics are a monitor of the saturation and crystallization of other REE-rich phases. This will probably be the case also for elements such as Y, Zr, Nb, Hf, Ta, Th and U.

A particular advantage of this approach to investigating accessory mineral saturation is that minerals that are not liquidus phases but that crystallize early from the bulk magma may still fractionate the REE from the melt and

affect the REE characteristics of far-from-liquidus phases, thus a relative paragenesis can be determined. A disadvantage of this approach is that it assumes that the process of magmatic differentiation operates relatively uninterrupted and that melt chemistries are not significantly augmented by processes such as assimilation and magma chamber replenishment.

For zircon, apatite and titanite from the BPZP, large abundance ranges within some crystal populations are interpreted as the result of *in situ* fractionation, where late crystallization ('localized saturation') in evolved intercumulus melt pools imparts trace element characteristics that diverge from those measured in earlier formed crystals. This is due to the melt pools having more evolved compositions and possibly lower temperatures, with consequent differences to mineral–melt K_d values. 'Seeing through' these variations within a population, differences are discernible between populations from different compositional zones within the BPZP. On average, the abundances of elements that substitute for the ESCs (e.g. P and Hf in zircon, and Mn and Y in titanite) increase in accessory minerals with magmatic differentiation. Assuming that the K_d values remained fairly constant or that they at least changed in the same direction for both ESC and substituting elements, this indicates that concentrations of the substituting elements were increasing in the melt with progressive differentiation. The decreasing abundances of Sr in apatite and titanite, and V in titanite, suggest decreasing abundances of these elements in the melt as a result of fractionation of feldspar (Sr), and magnetite, hornblende and biotite (V).

Apatite populations from felsic zones of the BPZP exhibit tightly clustered REE patterns relative to those observed from mafic zones (Fig. 8). This is taken to indicate apatite saturation in felsic zones, whereas in the mafic zones the compositions reflect *in situ* fractionation. The LREE slope and curvature for apatite change at the granodiorite–adamellite boundary (Fig. 10) as a result of relative depletion of La, Ce and Pr, which indicates saturation of allanite. This may be indicated also by the restricted U and Th abundances measured for both apatite and zircon. Normalized REE patterns of titanite further indicate LREE depletion of the melt, where progressively flatter patterns are measured with increasing differentiation. This probably reflects both allanite and apatite fractionation. Apatites from all zones except the diorite have curved HREE patterns as a result of fractionation of clinopyroxene, hornblende, biotite and perhaps zircon. A change in the enrichment trend of Y and the HREE in zircon (Fig. 7) is interpreted to represent zircon saturation in the bulk magma at the granodiorite–adamellite boundary (sample BP22, outer adamellite). This is consistent with saturation calculations (Fig. 15). The character of the Eu anomaly in zircon also changes at this point, from progressively increasing in mafic zones to smaller, more varied values in felsic zones. These features could occur because of 'localized saturation' of zircon in evolved intercumulus melt in mafic zones, and bulk magma saturation and crystallization in felsic zones. Titanite does not appear to have been an early crystallizing phase anywhere in the BPZP because the middle REE (MREE; Nd–Gd) abundances in both zircon and apatite are not observed to decrease relative to the HREE as would be expected for titanite saturation.

Comparison of measured and modelled whole-rock REE patterns

The saturation points of REE-enriched accessory minerals during differentiation of the Boggy Plain magma have been identified by the various methods (Table 3). Considering the advantages and pitfalls of each method, the following phases were probably significant REE fractionating phases within the BPZP: apatite in the granodiorite and all felsic zones; allanite and zircon in felsic zones. In addition, hornblende and biotite contribute to the behaviour of Y, Nb, Ba and the HREE in felsic zones.

Shown in Fig. 16 are chondrite-normalized measured and modelled REE patterns for BP22 (outer adamellite) and BP11 (inner adamellite). These two samples span a range from 65 to 72 wt % SiO_2, and lie on either side of a change in REE behaviour in the BPZP; whole-rock REE abundances increase from the diorite zone to BP22, but decrease from this point onwards with increasing differentiation (Fig. 3). Modelling was performed using the equations of DePaolo (1981) in two stages: (1) inner granodiorite (BP16) to outer adamellite (BP22); (2) outer adamellite to inner adamellite (BP11). The fractionating model mineral assemblage was constrained to contain only the significant REE fractionating phases identified in this study (Table 3) plus alkali-feldspar, plagioclase and clinopyroxene. The abundances of Yb and Lu in BP11 (inner adamellite) were reduced to correct for hydrothermal enrichment. The values were reduced until the chondrite-normalized HREE pattern became flat. The procedure for modelling both stages involved adjusting the proportions of biotite and feldspar to account for the Ba and Eu abundances, respectively, and 'fine-tuning' the other phases for the best fit to the measured abundances. The amount of fractional crystallization for each stage was within the limits imposed by major element modelling. Mineral–melt K_d values are from Sawka (1988) for apatite and allanite, from Hinton & Upton (1991) and Guo *et al.* (1996) for zircon, and from a compilation by Rollinson (1993) for all other phases.

Both modelled REE patterns exhibit a very good match to the measured whole-rock abundances. The BP22

Table 3: REE-enriched accessory minerals identified as early crystallized fractionating phases during differentiation of the Boggy Plain magma by four identifying methods

Identifier:	BP39 diorite	BP7 outer granodiorite	BP16 inner granodiorite	BP22 outer adamellite	BP11 inner adamellite	BP42 aplite
Euhedral morphology	apatite	apatite zircon	apatite zircon	allanite apatite zircon	allanite apatite zircon	allanite apatite zircon
'Inverse' modelling		apatite	apatite	apatite zircon	allanite apatite zircon	allanite apatite zircon
Saturation calculations (ap, zc, mon)*		apatite	apatite	apatite zircon	apatite zircon	apatite zircon
Mineral chemistry				allanite apatite zircon	allanite apatite zircon	allanite apatite zircon
Fractionating accessory phases:†		apatite	apatite	allanite apatite zircon	allanite apatite zircon	allanite apatite zircon
Other REE-enriched, early crystallized, fractionating phases:			hornblende biotite	hornblende biotite	biotite	

*Calculations based on saturation relationships determined by Watson & Harrison (1983), Harrison & Watson (1984), Rapp & Watson (1986) and Montel (1993). ap, apatite; zc, zircon; mon, monazite.
†Summary row. These minerals are considered to have crystallized early from the bulk magma and to have fractionated magma composition.

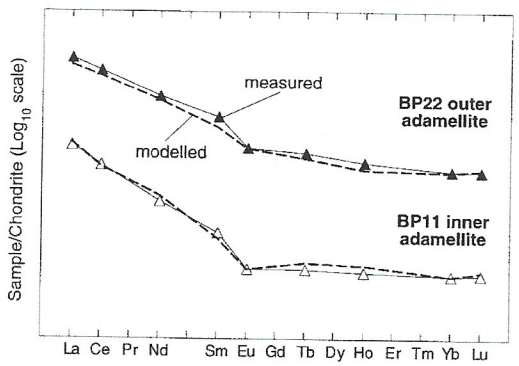


Fig. 16. Chondrite-normalized modelled (dashed lines) and measured (symbols and continuous line) whole-rock REE patterns for samples BP22 and BP11 from the adamellite zone of the BPZP. The modelled patterns are calculated from fractional crystallization of a model mineral assemblage constrained by petrography, 'inverse' modelling, saturation calculations and accessory mineral chemistry. The two sets of patterns are spaced on the *y*-axis for clarity.

pattern was modelled from the measured abundances of BP16 (inner granodiorite) by 10% fractional crystallization of a mineral assemblage containing 0·12 wt % calcic-amphibole, 12 wt % alkali-feldspar, 62 wt % plagioclase, 25 wt % clinopyroxene, 0·25 wt % biotite and 1·2 wt % apatite. To this assemblage was added ~1·8 wt % zircon to provide a better fit to the measured Hf abundance. Although this proportion is high, the addition of some zircon may be justified given the presence of xenocrystic zircon in felsic zones of the BPZP. The BP11 (inner adamellite) pattern, which represents a more evolved sample than BP22, was modelled from the measured abundances of BP22 by 90% fractional crystallization of an assemblage containing 22 wt % calcic-amphibole, 19 wt % alkali-feldspar, 37 wt % plagioclase, 4 wt % clinopyroxene, 17 wt % biotite, 0·13 wt % apatite, 0·1 wt % allanite and 0·19 wt % zircon. The abundances of Th and U were also modelled, but there is poor agreement (±19–50%) between measured and modelled values. Although these simple calculations only approximate the differentiation process

that operated in the Boggy Plain magma body, and do not account for *in situ* fractionation, there is reasonable agreement between the model mineral assemblages calculated here and actual modes estimated from thin-section point-counting (Wyborn, 1983). These calculations illustrate the good fit that can be obtained between measured and modelled REE patterns for selected granitoid samples by accurate identification of the saturation points of fractionating accessory phases.

Zircon: a special case?

A feature of the trace element chemistry of zircon from the BPZP is the monotony of its normalized REE pattern (Fig. 5). The shape of the zircon REE pattern does not change between populations, whereas there are systematic changes in the REE patterns of apatite, titanite and major rock-forming phases (Wyborn, 1983). Similarly, the abundances of individual REEs form ranges within a population that wholly or partially overlap the measured ranges for all other zircon populations (Fig. 6), whereas this is not the case for apatite or titanite.

These features of zircon chemistry are not unique to the BPZP. Zircon REE abundances and patterns analysed by Sawka (1988) from the McMurray Meadows Pluton also exhibit a very restricted range from rocks spanning granodiorite to leucogranite. In contrast to zircon in this pluton, allanite, titanite and other phases have systematically varying REE characteristics (Sawka *et al.*, 1984; Sawka, 1988). The 'constant compositions' of the zircons was interpreted by Sawka (1988) to indicate crystallization from essentially the same bulk magma composition. This cannot be the case for the BPZP because early crystallized zircon in the felsic zones fractionated from the evolving melt, and in mafic zones zircon crystallized in intercumulus melt pools. If the original Boggy Plain magma had a composition of ~60 wt % SiO_2, zircon may have crystallized over an interval of 15 wt % SiO_2. Other workers have reported the absence of significant chemical differences between zircon populations derived from different rock compositions (e.g. Rupasinghe & Dissanayake, 1987; Snyder *et al.*, 1993; Shannon *et al.*, 1997; Chesner, 1998).

One possible explanation could be a coincidence of interplay between changing abundances of REE (and other elements) in the melt and changing K_d values. This would require the REE composition of the evolving melt to have progressively decreased and K_d values to have increased at an equal rate to offset the REE abundance decreases in the melt. However, in felsic zones of the BPZP there are increasing Y + REE abundances in apatite and titanite, indicating that the melt was increasing in Y + REE abundance. It is improbable that zircon–melt K_d values were decreasing as differentiation proceeded in the BPZP adamellite and aplite zones.

Two recent experimental studies (Finch *et al.*, 2000; Hanchar *et al.*, 2000) of the 'xenotime' substitution mechanism for the incorporation of REE into zircon [$(Y, REE)^{3+} + P^{5+} = Zr^{4+} + Si^{4+}$] have revealed that there exist limits to the extent that 'xenotime' substitution may occur, and that the factors limiting the substitution are different for the LREE and HREE. The limit on REE concentrations in zircon is determined not to be a simple function of REE^{3+} ionic radii, but to depend in a complex way on structural strain at both the Zr octahedral site and the Si tetrahedral site. Specifically, the incorporation of the LREE into zircon is limited by strain at the Zr site, whereas HREE incorporation is limited by strain at the Si site caused by the substitution of P^{5+}, which has a significantly smaller ionic radius than Si^{4+}.

If 'xenotime' substitution is the only mechanism by which charge balance is maintained in REE-substituted zircon, then the atomic ratio of REE to P must be unity, and the abundance of the HREE in particular will be limited by the abundance of P and amount of lattice strain. The monotony of REE patterns and abundances for zircon from the BPZP may reflect REE and P 'saturation' of the crystal lattice.

A plot of Y + REE (atom) vs P (atom) reveals that for most BPZP zircons there is a significant deviation from a REE:P ratio of one, to REE > P (Fig. 17). The excess of REE over P indicates a more complex charge-balance mechanism, or multiple mechanisms. Other mechanisms could include exchange of OH^- groups for O^{2-} ions and coupled substitution at the Zr site (e.g. $REE^{3+} + Nb^{5+} = 2Zr^{4+}$), although measured abundances of elements such as Nb, Ta and V that may play a role in partial charge balance of excess REE are low (Appendix, Table A1). It is likely that more complex xenotime-type substitutions are involved, where the ratio of REE atoms to P atoms ranges up to 4:1 in zircon from BPZP mafic zones, and up to 2:1 in zircon from felsic zones. In zircons studied by Finch *et al.* (2000) and Hanchar *et al.* (2000), crystals with REE:P ratios greater than 1:1 maintain local charge balance by Li^+ and Mo^{6+} incorporation (from the crystal growth medium) into a distorted interstitial site 0·184 nm from four adjacent oxygen sites. In natural systems, four-coordinated major elements such as Mg, Al and Fe may enter this site [e.g. $^{[IV]}Al^{3+}$ has an ionic radius of 0·039 nm, and the sum of effective ionic radii for four-coordinated O^{2-} (0·139 nm) and Al^{3+} is 0·178 nm; Mg^{2+} and Fe will be slightly overbonded]. The incorporation of Li, Mg, Al and Fe cations into interstitial sites would maintain local charge neutrality according to the following substitutions:

REE:P 1:1, 'xenotime' substitution: $(Y, REE)^{3+} + P^{5+} = Zr^{4+} + Si^{4+}$ (Speer, 1982);

REE:P 2:1, $Li^+_{(int)} + 2(Y, REE)^{3+} + P^{5+} = 2Zr^{4+} + Si^{4+}$ (after Finch *et al.*, 2000);

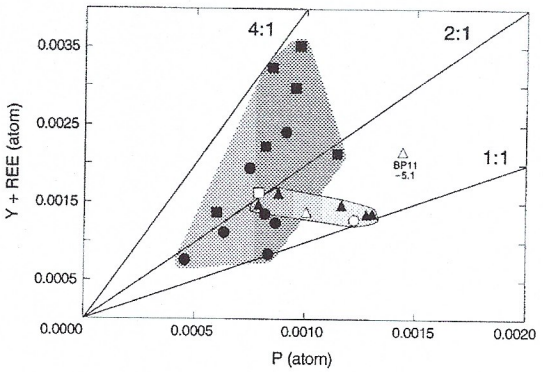


Fig. 17. Plot of Y + REE (atom) vs P (atom) for BPZP zircon. A one-to-one ratio of REE to P indicates substitution of REE and P into the zircon lattice by the 'xenotime' mechanism. REE to P (atom) ratios are indicated by continuous lines from the origin. Zircons from mafic zones of the BPZP are included in the dark grey shaded field; zircons from felsic zones are included in the light grey shaded field. Symbols are the same as for Fig. 5.

REE:P 3:1, $(Mg, Fe)^{2+}_{(int)} + 3(Y, REE)^{3+} + P^{5+} = 3Zr^{4+} + Si^{4+}$ (this study);

REE:P 4:1, $(Al, Fe)^{3+}_{(int)} + 4(Y, REE)^{3+} + P^{5+} = 4Zr^{4+} + Si^{4+}$ (this study).

Although Mg and Fe substitution into the Zr site and Al into the Si site cannot be ruled out, it is difficult to write substitution mechanisms including Mg and Fe that are constrained to have REE:P >1:1, and Al abundances in the Si site are likely to be negligible because of the large size mismatch between the two ions ($Al^{3+} \gg Si^{4+}$) and the relative inflexibility of the zircon lattice (Finch *et al.*, 2000). For BPZP zircon the average abundance of interstitial Al required to maintain charge balance is only 0·071 wt % Al_2O_3 (380 ppm Al), although significantly less would be required as a result of the presence of interstitial Li, Mg and Fe cations (Li, Appendix, Table A1; Mg and Fe, not analysed). The reported abundances of Al_2O_3, total-Fe and MgO in zircon are often above the limit of detection for EMP analysis, with abundances as high as the wt % level (Dickinson & Hess, 1982; Speer, 1982). Zircons from lower- to mid-crustal xenoliths with nearly identical REE characteristics to the BPZP zircons (Guo *et al.*, 1996; Sutherland *et al.*, 1998), having REE:P much larger than 1:1, contain up to 0·54 wt % Al_2O_3, 0·32 wt % total-Fe and 0·04 wt % MgO, enough to provide charge balance to the excess REE according to the mechanisms described above.

REE characteristics of BPZP zircon are interpreted to be a result of simple 'xenotime' and complex 'xenotime-type' substitutions, where REE not charge balanced by substituted P are charge balanced by Mg, Al, Fe, and possibly Li, present in interstitial sites. The increasing abundance of P in zircon with progressive magmatic differentiation (Fig. 7) indicates that P was increasing in the melt, and was increasingly available to charge balance the REE in zircon. In mafic zones of the BPZP, interstitial cations play a more dominant role in REE charge balancing. Nevertheless, it may remain a coincidence of melt crystallization processes and charge-balance requirements in zircon that imparts such similarity of REE characteristics to BPZP zircon, and other zircon populations (e.g. McMurray Meadows Pluton; Sawka, 1988).

Accessory minerals as petrogenetic indicators

Accessory mineral REE chemistry has been suggested by various workers to be a powerful tool in reconstructing whole-rock petrogenetic histories (e.g. Schaltegger *et al.*, 1999), or for distinguishing source-rock characteristics (Heaman *et al.*, 1990; Hinton & Upton, 1991; Nesbitt *et al.*, 1997). As petrogenetic indicators, accessory minerals are particularly useful for back-calculating the REE composition of the precipitating melt (Montel, 1993). The success of this procedure largely relies on the accuracy of K_d values and assumptions that the accessory mineral was a liquidus phase (or at least crystallized early) and that measured REE abundances reflect equilibrium partitioning from the melt. Accessory minerals in granitoid rocks have the potential to reveal subtle changes to melt composition (e.g. preserved as internal zoning) that are not preserved well or at all by major rock-forming phases or by whole-rock chemistry.

Average REE abundances for zircon and apatite from BP11 (inner adamellite) were used to back-calculate the REE composition of the precipitating melt (Fig. 18). This whole-rock sample was chosen because it is saturated for both accessory phases, its whole-rock composition is closer to a melt composition than for a mafic sample (it is ~70% trapped intercumulus liquid; Wyborn, 1983), and apatite from this sample has not been altered as in BP42 (aplite). The apatite-calculated melt resembles the whole-rock pattern, closely approximating both REE abundances and pattern. However, the zircon-calculated melt does not resemble either the apatite-calculated melt or the measured whole-rock pattern. This might be due to poorly constrained K_d values, although arbitrarily setting these so that the zircon-calculated pattern conforms to the BP11 whole-rock pattern would generate a zircon REE-K_d pattern that significantly differs from analytical and experimental (equilibrium) determinations (Watson, 1980; Mahood & Hildreth, 1983).

The changing REE abundances and patterns for apatite in the BPZP (Fig. 8) indicate that this mineral phase is potentially a useful petrogenetic indicator. This is not, however, the case for BPZP zircon, because REE abundances and patterns do not vary significantly (Fig.

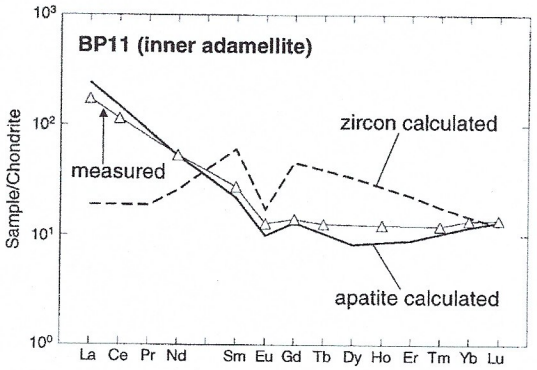


Fig. 18. Comparison of 'measured' and calculated melt compositions for BP11 (inner adamellite). The 'measured' value is the whole-rock composition, and the apatite and zircon modelled patterns represent average patterns calculated through appropriate mineral–melt K_d values [apatite values from Arth (1976); zircon values from Hinton & Upton (1991) and Guo *et al.* (1996)].

5) and therefore do not record evolving melt compositions (even though K_d values will change with whole-rock compositions, this will only increase or decrease calculated abundances, not change the overall pattern).

This result does not appear to be restricted to zircon from the BPZP. Zircon-calculated REE melt patterns for a range of published REE abundances in the literature sourced from intermediate–felsic plutonic and volcanic rocks, as well as some carbonatites and syenites, all yield similar patterns and abundances (data from, e.g. Gromet & Silver, 1983; Irving & Frey, 1984; Fujimaki, 1986; Heaman *et al.*, 1990; Barbey *et al.*, 1995; Bea, 1996; Hanchar & Hoskin, 1998). This clearly indicates that zircon REE characteristics are not as useful as other REE-rich accessory minerals as a petrogenetic monitor, and agrees with Maas *et al.* (1992), who found 'little systematic difference ... between zircons from different parent rocks' (p. 1292).

CONCLUSIONS

(1) Changes in the trace element chemistry of accessory zircon, apatite and titanite relate to changes in the bulk chemistry of the BPZP magma and the effect of localized saturation in trapped intercumulus melts. The REE chemistry of apatite and titanite in the adamellite and aplite reflects fractionation of the LREE from the magma by allanite. The increasing abundances of some trace elements in accessory phases (e.g. P, Sc, Nb in zircon; Mn, Ba, Hf in apatite; Mn, Y, Nb in titanite) from progressively more felsic samples reflects enrichment of the bulk magma in these elements. Large abundance ranges for individual trace elements in a single mineral population are a result of localized saturation in intercumulus melt pools.

(2) An integrated approach to identifying saturation points of accessory phases, involving 'inverse' modelling, saturation calculations and mineral chemistry, shows that these phases were saturated in the BPZP: inner granodiorite—apatite; outer and inner adamellite—allanite, apatite and zircon (plus hornblende and biotite); aplite—allanite, apatite, zircon (plus biotite).

(3) Zircons from the BPZP have chondrite-normalized REE patterns that show no variation with progressive whole-rock Si saturation. This is interpreted to be a result of simple 'xenotime' and complex 'xenotime-type' substitutions where REE not charge balanced by substituted P are charge balanced by Mg, Al and Fe in interstitial lattice sites.

(4) Changing apatite REE abundances and patterns, and successful back-calculation using mineral–melt K_d values to a 'melt' composition, for early-crystallized apatite indicate its potential use as a tracer of processes occurring during magma crystallization. The remarkable similarity both between BPZP zircon REE patterns and to published examples from a range of rock types indicates that zircon REE characteristics are generally not useful as an indicator of magmatic processes.

ACKNOWLEDGEMENTS

We thank the following persons for technical assistance: Steve Eggins, Nick Ware, Paul Sylvester, Ben Jenkins and Neil Gabittas. Ian Williams assisted in the field and with comments on an earlier draft. Janet Williams made a fantastic soup for supper. Mandy Hoskin is thanked for auxiliary assistance. We especially thank Professors Sven Maaløe, Urs Schaltegger and Kjell P. Skjerlie for constructive and thorough reviews, and Professor Kurt Bucher for efficient editorial oversight.

REFERENCES

Arth, J. G. (1976). Behaviour of trace elements during magmatic processes—a summary of theoretical models and their applications. *Journal of Research of the US Geological Survey* **4**, 41–47.

Bacon, C. R. (1989). Crystallisation of accessory phases in magmas by local saturation adjacent to phenocrysts. *Geochimica et Cosmochimica Acta* **53**, 1055–1066.

Barbey, P., Allé, P., Brouand, M. & Albarède, F. (1995). Rare-earth patterns in zircons from the Manaslu granite and Tibetan slab migmatites (Himalaya): insights in the origin and evolution of a crustally derived granite magma. *Chemical Geology* **125**, 1–17.

Bayly, M. B. (1965). The sampling error in modal analysis. *American Mineralogist* **50**, 196–211.

Bea, F. (1996). Residence of REE, Y, Th and U in granites and crustal protoliths; implications for the chemistry of crustal melts. *Journal of Petrology* **37**, 521–552.

Bea, F., Fershtater, G. & Corretgé, L. G. (1992). The geochemistry of phosphorus in granite rocks and the effect of aluminium. *Lithos* **29**, 43–56.

Bowring, S. A. & Williams, I. S. (1999). Priscoan (4·00–4·03 Ga) orthogneisses from northwestern Canada. *Contributions to Mineralogy and Petrology* **134**, 3–16.

Bowring, S. A., Erwin, D. H., Jin, Y. G., Martin, M. W., Davidek, K. & Wang, W. (1998). U/Pb zircon geochronology and tempo of the end-Permian mass extinction. *Science* **280**, 1039–1045.

Brueckner, H. K., Gilotti, J. A. & Nutman, A. P. (1998). Caledonian eclogite-facies metamorphism of Early Proterozoic protoliths from the North-East Greenland Eclogite Province. *Contributions to Mineralogy and Petrology* **130**, 103–120.

Buick, R., Thornett, J. R., McNaughton, N. J., Smith, J. B., Barley, M. E. & Savage, M. (1995). Record of emergent continental crust differs from 3·5 billion years ago in the Pilbara Craton of Australia. *Nature* **375**, 574–577.

Cameron, K. L. & Hanson, G. N. (1982). Rare earth element evidence concerning the origin of voluminous mid-Tertiary rhyolitic ignimbrites and related volcanic rocks, Sierra Madre Occidental, Chihuahua, Mexico. *Geochimica et Cosmochimica Acta* **46**, 1489–1503.

Chappell, B. W. (1996). Magma mixing and production of compositional variation within granite suites: evidence from the granites of southeastern Australia. *Journal of Petrology* **37**, 449–470.

Chappell, B. W. (1999). Aluminium saturation in I- and S-type granites and the characterisation of haplogranites. *Lithos* **46**, 535–551.

Chesner, C. A. (1998). Petrogenesis of the Toba Tuffs, Sumatra, Indonesia. *Journal of Petrology* **39**, 397–438.

Claoué-Long, J. C., Compston, W., Roberts, J. & Fanning, C. M. (1995). Two Carboniferous ages: a comparison of SHRIMP zircon dating with conventional zircon ages and $^{40}Ar/^{39}Ar$ analysis. In: *Geochronological Time Scales and Global Stratigraphic Correlation. SEPM Special Publication* **54**, 1–21.

Clark, A. M. (1974). A tantalum-rich variety of sphene. *Mineralogical Magazine* **39**, 605–607.

Compston, W., Williams, I. S. & Meyer, C. (1984). U–Pb geochronology of zircon from lunar breccia 73217 using a sensitive high mass-resolution ion microprobe. *Journal of Geophysical Research* **89**, Supplement, B525–B534.

Cuney, M. & Friedrich, M. (1987). Physicochemical and crystal-chemical controls on accessory mineral paragenesis in granitoids: implications for uranium metalogenesis. *Bulletin of Mineralogy* **110**, 235–247.

DePaolo, D. J. (1981). Trace element and isotopic effects of combined wallrock assimilation and fractional crystallization. *Earth and Planetary Science Letters* **53**, 189–202.

Dickinson, J. E., Jr & Hess, P. C. (1982). Zircon saturation in lunar basalts and granites. *Earth and Planetary Science Letters* **57**, 336–344.

Evans, O. C. & Hanson, G. N. (1993). Accessory-mineral fractionation of rare-earth element (REE) abundances in granitoid rocks. *Chemical Geology* **110**, 69–93.

Finch, R. J., Hanchar, J. M., Hoskin, P. W. O. & Burns, P. C. (2000). Rare earth elements in synthetic zircon. 2. A single-crystal X-ray study of xenotime substitution. *American Mineralogist* (in press).

Fujimaki, H. (1986). Partition coefficients of Hf, Zr, and REE between zircon, apatite, and liquid. *Contributions to Mineralogy and Petrology* **94**, 42–45.

Gaggero, L. & Gazzoti, M. (1996). Primary and secondary oxides, sulfides and accessory minerals in Mid-Atlantic gabbros: mineralogy and petrology. *Ofioliti* **21**, 105–116.

Green, T. H. & Pearson, N. J. (1986). Ti-rich accessory phase saturation in hydrous mafic–felsic compositions at high *P*, *T*. *Chemical Geology* **54**, 185–201.

Green, T. H. & Pearson, N. J. (1987). An experimental study of Nb and Ta partitioning between Ti-rich minerals and silicate liquids at high pressure and temperature. *Geochimica et Cosmochimica Acta* **51**, 55–62.

Gromet, L. P. & Silver, L. T. (1983). Rare earth element distributions among minerals in a granodiorite and their petrogenetic implications. *Geochimica et Cosmochimica Acta* **47**, 925–939.

Guo, J., O'Reilly, S. Y. & Griffin, W. L. (1996). Zircon inclusions in corundum megacrysts: I. Trace element geochemistry and clues to the origin of corundum megacrysts in alkali basalts. *Geochimica et Cosmochimica Acta* **60**, 2347–2363.

Hanchar, J. M. & Hoskin, P. W. O. (1998). Mud Tank Carbonatite, Australia, zircon. *Society for Luminescence Microscopy and Spectroscopy Newsletter* **10**, 2–3.

Hanchar, J. M. & Rudnick, R. L. (1995). Revealing hidden structures: the application of cathodoluminescence and back-scattered electron imaging to dating zircons from lower crustal xenoliths. *Lithos* **36**, 289–303.

Hanchar, J. M., Finch, R. J., Hoskin, P. W. O., Watson, E. B., Cherniak, D. J. & Mariano, A. N. (2000). Rare earth elements in synthetic zircon. 1. Synthesis, and rare earth element and phosphorus doping. *American Mineralogist* (in press).

Hanson, G. N. (1989). An approach to trace element modeling using a simple igneous system as an example. In: Lipin, B. R. & McKay, G. A. (eds) *Geochemistry and Mineralogy of Rare Earth Elements. Mineralogical Society of America, Reviews in Mineralogy* **21**, 78–97.

Hanson, G. N. & Langmuir, C. H. (1978). Modelling of major elements in mantle–melt systems using trace element approaches. *Geochimica et Cosmochimica Acta* **42**, 725–741.

Harrison, T. M. & Watson, E. B. (1983). Kinetics of zircon dissolution and zirconium diffusion in granitic melts of variable water content. *Contributions to Mineralogy and Petrology* **84**, 67–72.

Harrison, T. M. & Watson, E. B. (1984). The behaviour of apatite during crustal anatexis: equilibrium and kinetic considerations. *Geochimica et Cosmochimica Acta* **48**, 1467–1477.

Heaman, L. M., Bowins, R. & Crocket, J. (1990). The chemical composition of igneous zircon suites: implications for geochemical tracer studies. *Geochimica et Cosmochimica Acta* **54**, 1597–1607.

Hinton, R. W. & Upton, B. G. J. (1991). The chemistry of zircon: variations within and between large crystals from syenite and alkali basalt xenoliths. *Geochimica et Cosmochimica Acta* **55**, 3287–3302.

Hoskin, P. W. O. (1998). Minor and trace element analysis of natural zircon ($ZrSiO_4$) by SIMS and laser ablation ICPMS: a consideration and comparison of two broadly competitive techniques. *Journal of Trace and Microprobe Techniques* **16**, 301–326.

Hoskin, P. W. O. (2000). Patterns of chaos: fractal statistics and the oscillatory chemistry of zircon. *Geochimica et Cosmochimica Acta* **64**, 1905–1923.

Hoskin, P. W. O., Kinny, P. D. & Wyborn, D. (1998). Chemistry of hydrothermal zircon: investigating timing and nature of water–rock interaction. In: Arehart, G. B. & Hulston, J. R. (eds) *Water–Rock Interaction*. Rotterdam: Balkema, pp. 545–548.

Ireland, T. R. & Gibson, G. M. (1998). SHRIMP monazite and zircon geochronology of high-grade metamorphism in New Zealand. *Journal of Metamorphic Geology* **16**, 149–167.

Irving, A. J. & Frey, F. A. (1984). Trace element abundances in megacrysts and their host basalts: constraints on partition coefficients and megacryst genesis. *Geochimica et Cosmochimica Acta* **48**, 1201–1221.

Langmuir, C. H. (1989). Geochemical consequences of *in situ* crystallization. *Nature* **340**, 199–205.

Maaløe, S. & McBirney, A. R. (1997). Liquid fractionation; Part IV, Scale models for liquid fractionation of calc-alkaline magmas. *Journal of Volcanology and Geothermal Research* **76**, 111–125.

Maas, R., Kinny, P. D., Williams, I. S., Froude, D. O. & Compston, W. (1992). The Earth's oldest known crust: a geochronological and

geochemical study of 3900–4200 Ma old detrital zircons from Mt. Narryer and Jack Hills, Western Australia. *Geochimica et Cosmochimica Acta* **56**, 1281–1300.

Mahood, G. & Hildreth, W. (1983). Large partition coefficients for trace elements in high-silica rhyolites. *Geochimica et Cosmochimica Acta* **47**, 11–30.

McBirney, A. R., Baker, B. H. & Nilson, R. H. (1985). Liquid fractionation, part I. Basic principles and experimental simulations. *Journal of Volcanology and Geothermal Research* **24**, 1–24.

McDonough, W. F. & Sun, S.-S. (1995). The composition of the Earth. *Chemical Geology* **120**, 223–253.

Meurer, W. P. & Boudreau, A. E. (1998). Compaction of igneous cumulates, Part I: Geochemical consequences for cumulates and liquid fractionation trends. *Journal of Geology* **106**, 281–292.

Montel, J.-M. (1986). Experimental determination of the solubility of Ce-monazite in SiO_2–Al_2O_3–K_2O–Na_2O melts at 800°C, 2 kbar under H_2O-saturated conditions. *Geology* **14**, 659–662.

Montel, J.-M. (1993). A model for monazite/melt equilibrium and application to the generation of granitic magmas. *Chemical Geology* **110**, 127–146.

Muir, R. J., Ireland, T. R., Weaver, S. D. & Bradshaw, J. D. (1996). Ion microprobe dating of Paleozoic granitoids: Devonian magmatism in New Zealand and correlations with Australia and Antarctica. *Chemical Geology* **127**, 191–210.

Nesbitt, R. W., Hirata, T., Butler, I. B. & Milton, J. A. (1997). UV laser ablation ICP-MS: some applications in the Earth sciences. *Geostandards Newsletter: the Journal of Geostandards and Geoanalysis* **20**, 231–243.

O'Hara, M. J. & Fry, N. (1996*a*). The highly compatible trace element paradox—fractional crystallization revisited. *Journal of Petrology* **37**, 859–890.

O'Hara, M. J. & Fry, N. (1996*b*). Geochemical effects of small packet crystallization in large magma chambers—further resolution of the highly compatible element paradox. *Journal of Petrology* **37**, 891–925.

Owen, M. & Wyborn, D. (1979). Geology and geochemistry of the Tantangara and Brindabella 1:100 000 sheet areas. *Bureau of Mineral Resources, Geology and Geophysics, Australia, Bulletin* **204**.

Rapp, R. P. & Watson, E. B. (1986). Monazite solubility and dissolution kinetics: implications for the thorium and light rare earth chemistry of felsic magmas. *Contributions to Mineralogy and Petrology* **94**, 304–316.

Rollinson, H. R. (1993). *Using Geochemical Data: Evaluation, Presentation, Interpretation*. Singapore: Addison Wesley Longman, 352 pp.

Rønsbo, J. G. (1989). Coupled substitution involving REEs and Na and Si in apatite in alkaline rocks from the Ilimanaussaq intrusion, South Greenland, and the petrologic implications. *American Mineralogist* **74**, 869–901.

Rupasinghe, M. S. & Dissanayake, C. B. (1987). The geochemistry and mineralogy of zircons from Sri Lanka. *Bulletin of the Geological Society of Finland* **59**, 3–19.

Sawka, W. N. (1988). REE and trace element variations in accessory minerals and hornblende from the strongly zoned McMurry Meadows Pluton, California. *Transactions of the Royal Society of Edinburgh: Earth Sciences* **79**, 157–168.

Sawka, W. N., Chappell, B. W. & Norrish, K. (1984). Light-rare-earth-element zoning in sphene and allanite during granitoid fractionation. *Geology* **12**, 131–134.

Schaltegger, U. & Krähenbühl, S. (1990). Heavy rare-earth enrichment in granites of the Aar Massif (Central Alps, Switzerland). *Chemical Geology* **89**, 49–63.

Schaltegger, U., Fanning, C. M., Günther, D., Maurin, J. C., Schulmann, K. & Gebauer, D. (1999). Growth, annealing and recrystallisation of zircon and preservation of monazite in high-grade metamorphism: conventional and *in situ* U–Pb isotope, cathodoluminescence and microchemical evidence. *Contributions to Mineralogy and Petrology* **134**, 186–201.

Shannon, W. M., Barnes, C. G. & Bickford, M. E. (1997). Grenville magmatism in West Texas: petrology and geochemistry of the Red Bluff Granitic Suite. *Journal of Petrology* **38**, 1279–1305.

Smith, A. L. (1970). Sphene, perovskite and coexisting Fe–Ti oxide minerals. *American Mineralogist* **55**, 264–269.

Snyder, G. A., Taylor, L. A. & Crozaz, G. (1993). Rare earth element selenochemistry of immiscible liquids and zircon at Apollo 14: an ion probe study of evolved rocks on the Moon. *Geochimica et Cosmochimica Acta* **57**, 1143–1149.

Sparks, R. S., Huppert, H. E. & Turner, J. S. (1984). The fluid dynamics of evolving magma chambers. *Philosophical Transactions of the Royal Society of London, Series A* **310**, 511–534.

Speer, J. A. (1982). Zircon. In: Ribbe, P. H. (ed.) *Orthosilicates. Mineralogical Society of America, Reviews in Mineralogy* **5**, 67–112.

Sutherland, F. L., Hoskin, P. W. O., Fanning, C. M. & Coenraads, R. R. (1998). Models of corundum origin from alkali basaltic terrains: a reappraisal. *Contributions to Mineralogy and Petrology* **133**, 356–372.

Taylor, W. R., Esslemont, G. & Sun, S.-S. (1995). Geology of the volcanic-hosted Brockman rare-metals deposit, Halls Creek Mobile Zone, northwest Australia. II. Geochemistry and petrogenesis of the Brockman volcanics. *Mineralogy and Petrology* **52**, 231–255.

Vervoot, J. D., Patchett, P. J., Gehrels, G. E. & Nutman, A. P. (1996). Constraints on early Earth differentiation from hafnium and neodymium isotopes. *Nature* **379**, 624–627.

von Quadt, A., Günther, D., Frischknecht, R., Zimmermann, R. & Franz, G. (1997). The evolution of pre-Variscan eclogites of the Tauern Window (Eastern Alps): a Sm/Nd-, conventional and laser ICP-MS zircon U–Pb study. *Schweizerische Mineralogische und Petrographische Mitteilungen* **77**, 265–279.

Wark, D. A. & Miller, C. F. (1993). Accessory mineral behaviour during differentiation of a granite suite: monazite, xenotime and zircon in the Sweetwater Wash pluton, southeastern California, U.S.A. *Chemical Geology* **110**, 49–67.

Warner, S., Martin, R. F., Abdel-Rahman, A.-F. M. & Doig, R. (1998). Apatite as a monitor of fractionation, degassing, and metamorphism in the Sudbury Igneous Complex, Ontario. *Canadian Mineralogist* **36**, 981–999.

Watson, E. B. (1980). Some experimentally-determined zircon/liquid partition coefficients for the rare earth elements. *Geochimica et Cosmochimica Acta* **44**, 895–897.

Watson, E. B. & Harrison, T. M. (1983). Zircon saturation revisited: temperature and composition effects in a variety of crustal magma types. *Earth and Planetary Science Letters* **64**, 295–304.

Williams, I. S. (1998). U–Th–Pb geochronology by ion microprobe. In: McKibben, M. A. & Shanks III, W. C. & Ridley, W. I. (eds) *Applications of Microanalytical Techniques to Understanding Mineralizing Processes. Reviews in Economic Geology* **7**, 1–35.

Wolf, M. B. & London, D. (1994). Apatite dissolution into peraluminous haplogranitic melts: an experimental study of solubilities and mechanisms. *Geochimica et Cosmochimica Acta* **58**, 4127–4146.

Wyborn, D. (1983). Fractionation processes in the Boggy Plain zoned pluton. Ph.D. Thesis, Australian National University, 301 pp.

Wyborn, D., Turner, B. S. & Chappell, B. W. (1987). The Boggy Plain Supersuite: a distinctive belt of I-type igneous rocks of potential economic significance in the Lachlan Fold Belt. *Australian Journal of Earth Sciences* **34**, 21–43.

APPENDIX

Table A1: Microprobe trace element data (ppm) for zircon from the Boggy Plain zoned pluton, NSW, Australia†*

Analysis‡	Li	P	Ca	Sc	Ti	V	Mn	Y	Nb	La	Ce	Pr	Nd	Sm	Eu	Gd	Dy	Er	Tm	Yb	Lu	HfO_2§	Ta	Th	U
LA–(quadrupole) ICP-MS analyses																									
39-1.1		508		158				1804		0·11	16	0·2	3	7	1·3	37	145	265	56	497	102	2·36	0·7	345	465
39-2.1	1·3	388		133				1501			14	0·21	4	6	1·2	32	117	212	46	399	83	2·36	0·4	270	361
39-3.1	1·7	514	331	142	24	2	2	1116	0·7	0·10	12	0·13	2	4	0·7	18	88	166	36	338	70	2·40	0·5	188	298
39-4.1		281		106				996	1·5	0·22	14	0·11	1·1	3	0·8	18	82	149	31	292	59	2·37	0·5	198	297
39-5.1		561		134				3260	1·6	0·11	23	0·6	7	12	2·4	57	248	484	101	876	180	2·28	0·7	863	895
39-6.1	1	460	249	154	27	2	3	2593	1·7	0·13	20	0·4	6	11	2·0	53	211	382	80	706	142	2·72	0·6	549	607
39-8.1	0·6	531	242	131	17	1·5	1	1644	1·0	0·12	16	0·14	2·7	4	1·4	33	132	244	53	476	100	2·36	0·5	339	470
7-1.1	1·8	589	964	83	21	2	10	3976	2·6	5	46	1·8	14	16	3·0	85	342	579	119	1030	204	1·53	1·4	848	728
7-2.1		708	476	102	16	2		2866	2·3	0·08	33	0·5	7	12	2·1	62	239	409	85	745	150	1·81	1·2	549	590
7-2.2	0·9	371	428	80	13	0·6	1·6	1828	1·4	0·03	24	0·2	4	7	1·4	38	150	267	56	496	101	1·81	0·9	312	365
7-3.1	2·2	1379	1136	106		4		5514	5	3	71	2·0	20	23	4·1	114	451	764	158	1358	266	1·84	1·7	1246	1084
7-4.1	1·0	506	274	88	12	1	6	2996	2·2	1·1	46	0·8	8	12	2·4	65	248	416	86	742	147	1·88	1·0	577	580
7-8.1		602		84			5	4742	5	0·2	55	0·7	13	19	3·7	113	409	674	136	1165	226	1·65	1·4	1219	945
7-9.1	0·7	524	164	77	13	2	2·8	4329	4	0·10	52	0·9	11	19	3·2	91	361	636	131	1134	224	1·65	1·6	1168	1019
16-1.2		489		171			28	2076		0·9	71	0·8	4	7	1	37	163	308	70	659	137	3·89	3	526	908
22-2.1b		542		161				2118	1·4	0·12	42	0·3	7	15	4·4	66	201	301	62	578	113	2·39	0·9	271	290
22-2.1c		487		190				1921	4		44		8	16	4·4	62	181	284	56	527	106	2·73	1·4	280	338
22-4.1	2	808	420	168	31	2	1	1775	3	0·19	38	0·21	3·8	8	1·5	33	148	265	56	526	108	2·46	1·4	216	277
22-5.1	1·7	792	462	165	34	2	2	1767	2	1	38	0·5	5	7	1·8	36	146	260	55	516	104	2·29	1·2	205	259
22-7.1		722		157	36		12	1946	3	0·3	33	0·3	4	8	2·3	43	162	281	59	539	112	2·36	1·3	211	241
11-4.1	2	622	696	152	33	2	6	1781	4	0·2	52	0·2	1·6	7	1·6	31	143	268	59	559	112	2·36	2·0	290	423
11-5.1	3	892	493	251	75		4	2799	4		54	0·4	5	12	2·9	60	246	426	94	846	176	3·07	2·2	355	470
42-1.1		756		187				1669	2	0·2	35	0·3	2	7	2·1	35	150	246	56	490	101	2·83	1·3	164	219

Table A1: continued†

Analysis‡	Li	P	Ca	Sc	Ti	V	Mn	La	Ce	Pr	Nd	Sm	Eu	Gd	Tb	Dy	Ho	Er	Tm	Yb	Lu	HfO_2§	Th	U
SIMS (SHRIMP I) analyses																								
39-a.1								0·03	3·6	0·01	0·4	0·9	0·2	6·3	2·1	25	10	51	11	122	27			
39-b.1								0·05	5·7	0·09	2·6	5	0·7	21	6·2	67	26	127	26	270	59	2·36	264	352
39-c.1								0·03	4·9	0·04	1·0	2·1	0·4	12	3·9	44	18	84	18	193	42	2·40	458	499
39-d.1								0·02	4·4	0·01	0·5	1·2	0·3	8·2	2·4	29	11	55	12	125	27	2·37	91	163
39-e.1								0·07	8·3	0·13	3·8	6	1·0	30	9·5	108	46	218	44	462	100	2·28	480	570
39-f.1								0·03	6·3	0·08	2·6	5	0·8	23	6·9	73	28	127	26	269	55			
39-g.1								0·03	5·2	0·04	1·3	2·6	0·5	15	4·6	52	21	102	21	231	49	2·72	364	490
7-b.1								0·24	21	0·19	4·9	8·3	1·2	44	14	152	59	272	55	582	121	1·81	292	339
7-c.1								0·02	11	0·02	0·7	1·9	0·4	14	5·0	59	25	129	29	323	71	1·84	893	854
7-d.1								0·03	17	0·12	3·9	7·3	1·0	35	11	117	45	211	43	455	92	1·88	375	423
7-e.1								0·02	11	0·02	0·7	1·9	0·3	13	4·7	56	24	125	28	323	71	2·33	143	321
7-f.1								0·02	9·4	0·01	0·5	1·4	0·3	10	3·5	43	18	93	21	237	52	2·08	135	261
7-g.1								0·13	41	0·32	9	15	2·0	73	24	292	122	580	117	1191	246	1·65	1258	826
16-a.1								0·07	15	0·14	3·6	6	0·7	24	7·1	64	22	109	22	218	48			
16-b.1								0·05	3·5	0·04	1·2	3·0	0·2	19	6·5	66	25	131	27	277	61			
16-c.1								0·13	7·0	0·07	1·8	3·9	0·4	23	7·5	80	29	158	32	336	74			
16-d.1								0·05	3·7	0·03	0·7	2·2	0·3	18	7·3	90	36	204	43	449	102	0·39	4377	1959
16-e.1								0·07	25	0·05	1·0	2·2	0·5	15	4·9	52	20	135	30	325	76			
22-a.1								0·08	17	0·14	3·2	6	1·4	30	9·3	97	38	162	32	326	71	2·59	147	160
22-b.2								0·04	20	0·10	2·3	5	1·4	26	8·0	81	31	132	27	278	62			
22-b.3								0·03	16	0·05	0·7	1·5	0·5	9·3	3·0	33	13	60	13	143	33	2·73	164	198
22-c.1								0·03	14	0·05	0·6	1·5	0·4	10	3·3	38	15	75	16	173	30	2·45	74	121
22-d.1								0·04	18	0·07	1·3	2·8	0·7	15	4·8	51	20	104	22	237	52	2·46	105	149
22-e.1								0·03	13	0·05	0·9	2·1	0·6	12	4·3	49	20	94	20	222	52	2·29	102	151
22-f.1								0·02	12	0·04	0·3	0·7	0·2	5·2	1·6	18	7	44	10	120	29			

Analysis‡	Li	P	Ca	Sc	Ti	V	Mn	La	Ce	Pr	Nd	Sm	Eu	Gd	Tb	Dy	Ho	Er	Tm	Yb	Lu	HfO_2§	Th	U
11-a.2								0·03	15	0·05	0·7	1·7	0·5	11	3·8	41	16	83	16	176	39	3·17	121	170
11-a.3								0·05	15	0·05	1·4	2·8	0·8	18	6·1	65	26	129	27	288	68			
11-a.5								0·04	15	0·04	0·6	1·5	0·4	11	3·7	41	17	83	18	184	46			
11-c.1								0·11	15	0·02	0·6	1·3	0·3	8·9	2·7	35	15	50	17	182	44			
11-d.1								0·07	16	0·02	1·2	2·5	0·4	14	3·6	51	19	89	20	216	49			
11-e.1								0·07	16	0·01	1·3	2·6	0·7	15	3·2	50	19	102	22	241	57			
11-f.1								0·09	14	0·04	1·2	2·2	0·6	14	2·8	49	19	87	22	230	57			
42-a.1								0·09	15	0·14	0·9	2·1	0·6	14	4·7	50	20	107	21	225	53	2·83	90	154
42-b.1								0·06	16	0·11	1·0	2·2	0·4	12	4·1	41	16	83	16	174	39	3·42	166	251
42-b.2								0·06	19	0·16	1·5	4·1	0·5	31	12·9	149	63	346	70	773	177	3·98		
42-c.1								0·06	14	0·08	1·3	2·4	0·5	14	4·5	44	17	90	18	186	41	3·16	145	182
42-d.2								0·23	22	0·12	2·0	3·2	1·1	18	6·6	71	31	177	38	452	113			

*For LA–ICP-MS data a blank space indicates abundance below the limit of detection; for SIMS data a blank space indicates 'not analysed'.
†Acquired by both laser ablation quadrupole ICP-MS analysis (session 1, 5 August 1997; session 2, 8–9 August 1997) and SIMS analysis (SHRIMP I, ANU). SIMS REE analyses were performed during December 1989 to February 1990; SIMS Hf, Th and U analyses were performed during October 1996 to December 1996.
‡All analyses prefixed by 'BP'; whole-rock samples: BP39, diorite; BP7, outer granodiorite; BP16, inner granodiorite; BP22, outer adamellite; BP11, inner adamellite; BP42, aplite.
§Given as wt % oxide; LA–ICP-MS data reduced using Hf as the internal reference—Hf abundance measured by SIMS analysis.

Table A2: Microprobe trace element data (ppm) for apatite from the Boggy Plain zoned pluton, NSW, Australia†*

Analysis‡	Li	Si	Sr	Y	Nb	Ba	La	Ce	Pr	Nd	Sm	Eu	Gd	Dy	Er	Tm	Yb	Lu	Hf	Ta	Th	U
39-1.1		1321	522	605		6·9	729	1627	213	920	169	15·2	154	108	52	6·2	34	4·5	0·07	0·01	27	17·8
39-2.1		930	521	695		7·0	684	1676	233	1046	204	15·8	188	128	59	6·7	36	4·7			15·4	5·3
39-4.1		1967	524	652		7·6	732	1733	232	1004	191	14	178	120	57	6·6	36	4·6	0·1	0·01	17·3	6·9
39-5.1		976	506	677		7·4	702	1672	230	1016	196	15	180	120	55	6·4	35	4·4	0·07	0·01	27	12·5
39-6.1		2005	515	529		8	713	1510	184	793	144	15	138	96	46	5·6	32	4·3	0·11	0·01	70	78
39-7.1		2237	544	470		7	772	1611	194	800	144	16·2	132	83	40	4·9	27	3·5	0·06	0·01	17	6·9
39-8.1		1117	547	701		7·6	680	1645	229	1004	198	16	186	126	57	6·8	37	4·5	0·07		15·7	5·3
39-9.1		2075	544	726		7·7	735	1758	240	1056	205	17	193	129	59	6·7	35	4·5	0·11	0·02	18	5·3
7-1.1	1·2		609	378	0·16	9	1215	2304	261	1003	155	14	131	79	36	4·4	25	3·5		0·01	16	6·1
7-2.1		1504	464	314	0·09	8·8	1393	2267	222	754	110	12·3	86	55	29	3·8	21	3·6	0·06		42	16·7
7-2.1a		3931	524	328	0·23	3	1534	2462	243	845	121	14·0	92	61	30	4·1	24	3·6			40	22
7-3.1a		1658	479	568	0·18	10·3	1414	2711	313	1232	201	14·3	172	111	50	5·9	33	4·6			25	8
7-4.1	4·1	14776	528	562	0·4	16	959	2003	257	1100	200	10·2	168	104	46	5·1	27	3·3	0·10	0·04	23·0	10·5
7-5.1			536	461		4	1154	2149	258	1049	176	11·1	153	92	39	4·7	25	3·7	0·5	0·02	18	8
7-6.1			508	457		8	1184	2280	274	1083	177	11	145	89	39	4·5	24	3·3	0·07	0·01	23	13·5
7-7.1		20103	518	381	0·6	31	1260	2261	244	900	136	12·5	110	70	34	4·4	25	3·6	0·4		31	16
16-1.1	1·1	1060	451	317		11·4	1635	2997	304	1039	138	13·4	104	60	29	4·0	24	3·4		0·01	33	20
16-2.1	1·1	735	462	262		9·6	1452	2588	257	839	109	12	75	45	23	2·9	19	2·8			25	22
16-3.1	1·2	533	438	195		7·9	1132	2028	203	669	85	8·6	63	35	17	2·2	13	2·1	0·07		14	9·2
16-5.1	1·9	1143	508	331		11·3	1684	3097	327	1117	151	13·1	113	63	29	3·5	22	3·1		0·01	33	17·2
16-6.1	1·4	808	567	266		9·7	1366	2498	277	968	133	9·9	102	52	22	2·6	14·3	2·2	0·07	0·01	14	12
16-7.1	1·5	1188	508	239		9·9	1332	2384	246	829	110	10·6	80	44	20	2·5	15	2·3			11·1	6·4
16-8.1	1·0	519	472	218		8·2	1158	2105	219	736	94	9·6	68	39	20	2·7	17	2·6		0·01	14	15
16-9.1	3·1	1099	475	237		10·1	1339	2401	251	883	119	11	89	45	22	2·6	16	2·3	0·08	0·01	17·0	14·3
16-10.1	2·3	1727	467	397		23	2131	3921	403	1403	185	17·7	135	77	37	4·8	28	4·3	0·07	0·01	38	11·4
16-11.1		359	489	204		9·2	1333	2335	236	790	99	10·5	71	38	18	2·3	14·3	1·9		0·01	12·8	9·2

Analysis‡	Li	Si	Sr	Y	Nb	Ba	La	Ce	Pr	Nd	Sm	Eu	Gd	Dy	Er	Tm	Yb	Lu	Hf	Ta	Th	U
22-3.1	1·1	1528	264	524		10·2	1208	2818	350	1336	199	15	150	90	45	5·9	36	5·2		0·01	20·5	7·0
22-4.1	1·6	2052	286	481		11·1	1266	2877	352	1358	201	15·4	145	87	42	5·4	32	4·6		0·01	19	5·4
22-5.1	2·7	1840	310	469		10·7	1263	2879	338	1255	175	14·9	132	78	41	5·3	33	4·8			17·5	4·5
22-6.1	2·1	1500	284	501		10·1	1197	2743	336	1282	192	15·0	138	87	44	6·0	37	5·5	0·07	0·01	22·8	6·2
22-7.1	2·9	1879	264	498		10·5	1167	2763	347	1337	204	16	153	91	46	5·9	36	5·3	0·07		26	8·1
22-8.1	2·1	1353	348	526		12·3	1482	3286	400	1534	235	17	184	102	46	5·8	32	4·6			17·3	4·7
11-1.1	1·7	1585	366	771		14·0	1717	3784	453	1734	260	19	191	130	66	8·9	56	8·2	0·10	0·02	33	8·3
11-2.1	0·9	2222	284	690	0·32	14	1578	3448	411	1515	216	18·0	153	105	56	7·5	49	7·0	0·10	0·01	38	10·3
11-3.1	1·1	1517	294	793	0·20	11·8	1370	3098	388	1488	246	17	185	128	65	8·5	53	7·5		0·01	26·5	7·2
11-4.1	2·1	697	306	583		9·8	1135	2680	335	1251	192	17·8	139	93	49	6·9	43	6·1			31	8·4
11-5.1	1·6	1346	270	681		11·0	1330	2916	344	1231	189	15·2	136	102	54	7·7	47	7·1	0·07	0·01	23	5·5
11-6.1	1·9	1470	227	787		10·9	1399	3016	349	1234	197	15·5	139	111	62	8·8	57	8·1	0·07		34	9·0
11-7.1	1·7	1486	264	804		11·0	1298	2948	365	1410	227	17	170	127	66	9·2	57	8·4	0·08		29	6·9
11-8.1	3·1	2647	366	501		13	1807	3759	415	1429	185	17·8	123	82	40	5·6	35	4·9	0·07	0·02	30	8·0
11-9.1	2·5	1318	380	490	0·14	10·5	1255	2833	339	1218	176	18·0	123	82	41	5·5	34	4·8	0·07		23·1	6·4
11-10.1	3·0	1191	362	446		11·9	1489	3123	346	1189	160	14·2	111	73	38	5·2	31	4·5	0·07		18·7	4·7
42-3.1	2·7	1334	183	1192	0·2	9·8	1119	2777	352	1289	227	20·4	184	178	94	15·5	108	15·3	0·08	0·03	37	12·3
42-6.1	4·3	1512	195	1316	0·2	12·6	1508	3432	403	1431	224	18	164	167	103	17·7	134	20	0·07	0·02	40	10·1
42-8.1	3·0	1643	158	1289	0·2	12·6	1493	3346	399	1423	236	18·0	175	171	99	16·5	122	18	0·06	0·03	37	10·2
42-10.1	2·2	1332	248	1627	0·4	10·1	1292	2771	332	1183	231	17·0	199	224	119	18·0	123	16·6	0·07	0·03	29	7·6

*A blank space indicates abundance below the limit of detection (Sc below limits of detection in all analyses).
†Acquired by laser ablation quadrupole ICP-MS during analytical sessions 1 (5 August 1997) and 2 (8–9 August 1997); data reduced using Ca as the internal reference (CaO = 55·6 wt %).
‡All analyses prefixed by 'BP'; whole-rock samples: BP39, diorite; BP7, outer granodiorite; BP16, inner granodiorite; BP22, outer adamellite; BP11, inner adamellite; BP42, aplite.

Table A3: Microprobe trace element data (ppm) for titanite from the Boggy Plain zoned pluton, NSW, Australia†*

Analysis‡	P	Sc	V	Mn	Sr	Y	Zr	Nb	La	Ce	Pr	Nd	Sm	Eu	Gd	Dy	Er	Tm	Yb	Lu	Hf	Ta	Th	U
16-3.1	91	14	1774	489	20	646	204	109	533	1494	201	799	164	29	125	117	65	10	70	10·1	15·9	8·4	16·0	20
16-4.1	397	18	1229	777	29	570	509	83	1157	2712	319	1071	171	80	115	95	57	8·9	66	10·3	50	19	21	105
16-6.1	108	9	1200	724	27	569	275	85	975	2477	294	991	161	58	108	93	55	9·2	70	11·0	19	8·4	22	53
22-1.1	215	10	1060	877	17	414	414	1178	1448	5010	727	2759	482	105	354	310	191	—	227	36	28	16·5	312	300
22-2.1	317	15	1068	1013	18	887	887	2830	1789	7523	1252	5155	1061	112	763	716	427	—	464	61	124	542	412	151
22-3.1	215	13	1179	911	22	652	652	2164	2094	9504	1635	7235	1592	180	1159	1065	583	—	567	69	63	337	619	135
22-4.1	368	8	915	800	20	1387	1387	1659	1730	5569	757	2832	485	111	360	313	189	—	232	37	134	45	513	406
22-5.1	97	14	1081	792	17	400	400	571	1006	3295	460	1726	308	69	235	202	121	—	140	22	35	8·6	175	176
22-6.1	420	15	1207	715	22	384	384	1372	1131	4752	828	3797	874	166	747	668	361	—	345	48	26	24	470	494
22-7.1	497	12	989	987	26	1265	1265	4052	3271	10495	1362	4824	758	173	530	450	281	—	346	55	64	32	979	1337
22-8.1	130	13	1032	745	16	285	285	600	764	2675	400	1636	339	65	277	250	138	—	144	22	33	16·6	138	140
11-1.1	138	32	812	1158	7	350	350	2553	1049	4722	876	4100	1087	134	988	977	564	87	609	89	49	92	155	252
11-2.1	155	32	793	1198	5·7	647	647	4548	1371	6500	1304	6508	1933	122	1780	1779	955	145	972	131	77	759	210	290
11-3.1	160	35	837	1212	7	447	447	3435	1311	6589	1359	6926	2080	148	1911	1906	1045	157	1041	138	53	281	217	302
11-4.1	132	31	814	1107	6·2	353	353	1827	867	3775	692	3203	861	122	792	780	451	69	479	71	76	67	119	201
11-6.1	150	35	809	1166	7·1	453	453	3605	1277	6054	1186	5837	1615	145	1459	1418	806	123	831	113	61	201	195	295
11-7.1	156	33	861	1138	6·9	368	368	2285	1027	4347	776	3582	903	137	815	799	468	72	513	76	47	55	163	263
11-8.1	141	34	827	1213	5·9	513	513	3719	1502	6920	1312	6273	1707	126	1522	1497	835	127	852	119	64	294	216	304
11-10.1	92	36	810	1188	6	383	383	3064	1121	5288	1001	4918	1348	142	1207	1196	702	108	746	108	56	164	165	256

*A blank space indicates abundance below the limit of detection (Ba below limits of detection in all analyses); —, not analysed.
†Acquired by laser ablation quadrupole ICP-MS during analytical sessions 1 (5 August 1997) and 2 (8–9 August 1997); data reduced using Ca as the internal reference (CaO = 28·6 wt %).
‡All analyses prefixed by 'BP'; whole-rock samples: BP16, inner granodiorite; BP22, outer adamellite; BP11, inner adamellite.